frontiers

Coherence and coupling functions reveal microvascular impairment in treated hypertension

Valentina Ticcinelli [1], **Tomislav Stankovski** [1,2], **Dmytro Iatsenko** [1,3], **Alan Bernjak** [1,4], **Adam E. Bradbury** [1], **Andrew R. Gallagher** [5], **Peter B. M. Clarkson** [6], **Peter V. E. McClintock** [1] **and Aneta Stefanovska** [1*]

[1] *Lancaster University, Physics Department, Lancaster, United Kingdom*
[2] *Ss. Cyril and Methodius University, Faculty of Medicine, Skopje, Macedonia*
[3] *Deutsche Bank AG, London, United Kingdom*
[4] *University of Sheffield, Department of Oncology & Metabolism, Sheffield, United Kingdom*
[5] *Lancaster Medical Practice, Lancaster, United Kingdom*
[6] *Raigmore Hospital, Cardiology Department, Inverness, United Kingdom*

Correspondence*:
Aneta Stefanovska
aneta@lancaster.ac.uk

ABSTRACT

The complex interactions that give rise to heart rate variability (HRV) involve coupled physiological oscillators operating over a wide range of different frequencies and length-scales. Based on the premise that interactions are key to the functioning of complex systems, the time-dependent deterministic coupling parameters underlying cardiac, respiratory and vascular regulation have been investigated at both the central and microvascular levels. Hypertension was considered as an example of a globally altered state of the complex dynamics of the cardiovascular system. Its effects were established through analysis of simultaneous recordings of the electrocardiogram, respiratory effort, and microvascular blood flow (by laser Doppler flowmetry). The signals were analysed by methods developed to capture time-dependent dynamics, including the wavelet transform, wavelet-based phase coherence, nonlinear mode decomposition and dynamical Bayesian inference, all of which can encompass the inherent frequency and coupling variability of living systems. Phases of oscillatory modes corresponding to the cardiac (around 1.0 Hz), respiratory (around 0.25 Hz) and vascular myogenic activities (around 0.1 Hz) were extracted and combined into two coupled networks describing the central and peripheral systems respectively. The corresponding spectral powers and coupling functions were computed. The same measurements and analyses were performed for three groups of subjects: healthy young (Y group, 24.4$\pm$3.4 y), healthy aged (A group, 71.1$\pm$6.6 y), and aged treated hypertensive patients (ATH group, 70.3$\pm$6.7 y). It was established that the degree of coherence between low-frequency oscillations near 0.1 Hz in blood flow and in HRV time series differs markedly between the groups, declining with age and nearly disappearing in treated hypertension. Comparing the two healthy groups it was found

that the couplings to the cardiac rhythm from both respiration and vascular myogenic activity decrease significantly in aging. Comparing the data from A and ATH groups it was found that the coupling from the vascular myogenic activity is significantly weaker in treated hypertension subjects, implying that the mechanisms of microcirculation are not completely restored by current anti-hypertension medications.

Keywords: hypertension, cardiovascular regulation, ageing, heart rate variability, microvascular blood flow oscillations, vascular myogenic activity, nonlinear oscillator, wavelet transform, coherence analysis, Bayesian inference, coupling functions

1 INTRODUCTION

The complex variation in the human heart rate, well known as heart rate variability (HRV), has been studied extensively over the years (Billman, 2011). Although (Hales, 1733) had noted that the heart rate varied with respiration, known today as respiratory sinus arrhythmia (RSA), and (Ludwig, 1847) had already recorded RSA more than one-and-a-half centuries ago, the physiological origin of the processes involved in the frequency modulation of the heart rate is still widely disputed. Based on spectral analysis methods with linear frequency resolution, a ratio between low frequencies (usually linked with the activity of the sympathetic nervous system) and high frequencies (usually linked with parasympathetic activity) was proposed as a measure of health (Malliani et al., 1991; Pagani et al., 1986). This concept was subsequently disputed as greatly oversimplifying the complex non-linear interactions between the sympathetic and parasympathetic divisions of the autonomic nervous system (Eckberg, 1997) and it is now clear that the LF/HF ratio does not accurately measure cardiac sympatho-vagal balance (Billman, 2011).

Other approaches came from statistical physics and scaling properties (Amaral et al., 1998; Bernaola-Galván et al., 2001), multifractal properties (Ivanov et al., 1999), and 1/f spectra (Ivanov et al., 2001; Kobayashi and Musha, 1982) which were all proposed as ways of characterising HRV. A reduction of variation was associated with sudden cardiac death and the Research Resource for Complex Physiologic Signals was created under the auspices of the National Center for Research Resources of the National Institutes of Health, intended to stimulate current research and new investigations in the study of cardiovascular and other complex biomedical signals (Goldberger et al., 2000).

Much of the HRV seems to be of deterministic origin, arising through a complicated interaction between physiological oscillations occurring on a wide range of different time scales (Bashan et al., 2012; Stefanovska, 2007). A promising approach, therefore, is to extract the deterministic features of the signals as far as possible, paying close attention to the nonlinear and time-dependent dynamics of the parameters of cardiovascular regulation and in particular to the *coherence* and *coupling functions* between oscillatory components (Clemson and Stefanovska, 2014; Clemson et al., 2016; Sheppard et al., 2012; Smelyanskiy et al., 2005; Stankovski et al., 2012; Stefanovska and Bračič, 1999; Stefanovska et al., 2000). Moreover, we hypothesise that additional understanding might be gained by investigating the oscillatory components of signals measured at different sites of the cardiovascular system. In what follows we apply these approaches to gain insight into two particular states of the body that often co-exist in practice: ageing and hypertension.

Because the functioning of the cardiovascular system is closely related to its efficiency in adapting to a time-varying environment, the couplings between its oscillating components could reveal its overall health. One aspect of ageing is the progressive physiological weakening of the links that keep the cardiovascular system reactive and functional. This is why changes in the cardiovascular network with ageing have been extensively investigated (Agelink et al., 2001; Antelmi et al., 2004; Jensen-Urstad et al., 1997; Kelly et al., 1995; Levy, 2001; Shiogai et al., 2010). As well as compromising the tone (Kelly et al., 1995) and elasticity

(Levy, 2001) of the blood vessels, ageing reduces HRV (Agelink et al., 2001; Antelmi et al., 2004; Shiogai et al., 2010) probably due to a weakening in couplings (Iatsenko et al., 2013).

Established hypertension can arise at any time of life, but predominantly occurs in the older age group, affecting about 40% of those over 25 (World Health Organisation, 2013). It is usually associated with an increase in the total peripheral resistance to blood flow, which contributes to high pressure while the cardiac output still remains normal. Many mechanisms have been proposed to account for the raised peripheral resistance. They include disturbances in renin-angiotensing system regulation, abnormalities of the sympathetic nervous system (Guyenet, 2006; McCurley et al., 2012), endothelial dysfunction (Taddei and Bruno, 2016), presence of specific genes expressed within the smooth muscle (Bai et al., 2013) and endothelial cells (Messaoudi et al., 2015), and vascular inflammation (Harvey et al., 2015). There is an associated loss of elasticity of the vessel walls accompanied by a reduction in their radii (Feihl et al., 2006). Hypertension is considered to be a major risk factor for heart disease, stroke and kidney failure and leads to premature death and disability (World Health Organisation, 2013). Currently available treatments that successfully reduce blood pressure also claim to revert the associated microvascular dysfunctions such as rarefaction and loss of reactivity (Sörös et al., 2013; Taddei et al., 2000).

Quite generally, the health and functionality of the human cardiovascular system can be assessed through the analysis of its associated signals, such as blood pressure and electrocardiogram (ECG). Heart rate variability (HRV, derived from the ECG) and blood pressure, analysed in the time and frequency domains, have both diagnostic and prognostic value for essential hypertension (Malik, 1996; Verdecchia et al., 1994). The diagnostic and prognostic potential of skin blood flow, measured by laser-Doppler flowmetry (LDF), has taken longer to become generally appreciated (Rossi et al., 2011; Virdis et al., 2014). Several oscillatory components can be detected in LDF signals, of which the three fastest ones are (Bernardi et al., 1997; Bernjak et al., 2012; Shiogai et al., 2010; Söderström et al., 2003; Stefanovska et al., 1999; Stefanovska, 2007): cardiac (0.6–2 Hz, usually $\approx$ 1 Hz); respiratory (0.145–0.6 Hz, usually $\approx$ 0.25 Hz) and myogenic (0.052–0.145 Hz, usually $\approx$ 0.1 Hz). These oscillations are similar to those observed in HRV (Lotrič et al., 2000) and blood pressure (Stefanovska and Bračič, 1999). The 0.1 Hz oscillation corresponds to so-called Mayer waves (Julien, 2006) in blood pressure or so-called LF waves in HRV (Malik, 1996).

While the origins and nature of the cardiac and respiratory (known as HF in HRV) oscillations are generally agreed (Eckberg, 2003; Saul et al., 1991), the attribution of the mechanism underlying the 0.1 Hz oscillation differs, depending on whether it is being observed in cardiac or vascular activity. Studies of HRV and blood pressure variability emphasize the involvement of sympathetic nerve activity in oscillations around 0.1 Hz (Julien, 2006; Malpas, 2002), which are currently mainly attributed to time-delays in the baroreflex feedback loop. Qualitatively, changes in pressure are felt by baroreceptors that provide information continuously to the spinal cord. In response, appropriate sympathetic stimuli are generated and transmitted to all vascular beds and to the heart, aimed at maintaining the pressure within certain limits. Due to the finite response times, this sympathetic "correction" arrives after a delay, resulting in self-sustained oscillations. In contrast, studies of vascular dynamics mostly attribute 0.1 Hz oscillations to spontaneous movements of smooth muscle in the vessel wall, also known as myogenic activity, or Bayliss effect, or vasomotion. While the mechanism is not yet completely understood, it involves the opening and closing of ion channels in the endothelial and smooth muscle cells in the vessel walls (Aalkjaer and Nilsson, 2005) in response to changes in blood pressure. These vascular dynamical processes can be investigated through blood flow measurements.

Armed with the new method of time-localised wavelet phase coherence analysis (Sheppard et al., 2012) we have investigated the coherence between 0.1 Hz oscillations in HRV and LDF blood flow (also referred

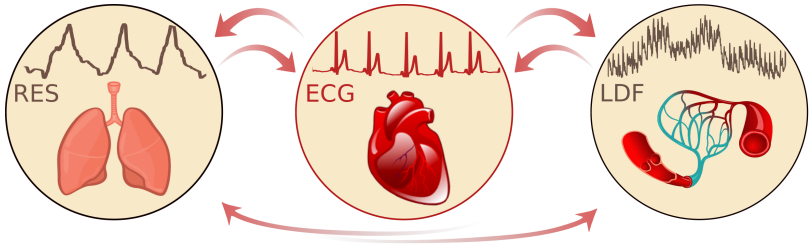

Figure 1. Schematic representation of the interactions between respiratory, cardiac and vascular activity, together with the corresponding recordings: respiratory effort signal (RES), electrocardiogram (ECG) and laser Doppler flowmetry (LDF).

to as skin blood flow, or SBF) in order to establish how it changes with age and in treated hypertension. Furthermore, based on 30-min resting-state simultaneous recordings of the electrocardiogram (ECG), respiratory effort signal (RES) and LDF blood flow signal, the couplings between cardiac, respiratory and microvascular activity were investigated, as indicated in Fig. 9.

Nonlinear mode decomposition (NMD) (Iatsenko et al., 2015) was used to extract the phases of the corresponding physiological modes. The instantaneous phase (frequency) was extracted individually around the subject's own characteristic rhythms, as found by wavelet transform. NMD was applied to extract the modes from the signals shown in Fig. 9, both directly at source and from the LDF. Two networks of interacting oscillators were analysed:

- *Central network*: cardiac from ECG (ϕ_C), respiration from RES (ϕ_R) and myogenic from LDF (ϕ_m);
- *Peripheral network*: cardiac (ϕ_c), respiration (ϕ_r) and myogenic (ϕ_m) all from LDF.

The first network describes the phase dynamics between the oscillations at their sources (indicated by subscript upper-case letters). Hence, the oscillations have different spatial origin. The second network describes how the couplings propagate into the blood flow (subscript lower-case letters). All three oscillations are detected in the same position in the microvasculature.

In this paper we apply these advanced methods to provide a comprehensive analysis of oscillatory interactions. It enables us to investigate the effects of ageing and treated hypertension on cardiovascular dynamics, at both the central and peripheral levels. First, however, as essential physiological background, we provide a more detailed description of the oscillations themselves.

1.1 Background: Cardiovascular oscillations

The vascular network, the system of arteries, arterioles, capillaries, venules and veins provides every cell of the human body with oxygen and nutrients, and carries away the waste metabolites. Cellular needs are dependent on the activity that the individual is performing, on the environmental conditions, on the health of the individual, and hence on time. Thus the cardiovascular system must be able to respond to time-dependent changes: centrally, the respiration and heart rates change significantly accordingly to need (Saul et al.,1991), and are coupled to each other. The modulation of heart rate by the frequency of respiration is known as respiratory sinus arrhythmia (RSA) (Clynes, 1960). This modulation is easy to observe by simultaneous recordings of the ECG and respiratory effort and has frequently been reported to change with age (see e.g. (Iatsenko et al., 2013)) and cardiovascular diseases. However, as mentioned above, the mechanisms of physiological coupling that enable this modulation are not yet settled and remain a matter of intensive investigation.

Oscillation	Characteristic frequency (Hz)	Range (Hz)
cardiac	1	0.6–2.0
respiratory	0.25	0.145–0.6
myogenic	0.1	0.052–0.145

Table 1. The oscillations analysed

Oscillations spanning a wide frequency range have also been observed in recordings from the microvasculature (Bertuglia et al., 1994; Johnson, 1991; Karstrup et al., 1989; Stefanovska et al., 1999). They occur at a number of characteristic frequencies, of which the three relevant to the present work are summarised in Table 1. We now consider them each individually.

Cardiac and respiratory oscillations

The heart rhythmically pumps blood into the vascular system, and the corresponding oscillations propagate to the capillary bed, where they can be detected in skin blood flow by laser Doppler flowmetry (LDF) (Bernardi et al., 1997; Rossi et al., 2006).

The respiratory (RES) activity of the lungs generates a wave of pressure that is propagating in the vascular network and can be detected even in the microvasculature using LDF (Bollinger et al., 1991; Hoffman et al., 1990; Stefanovska and Hožič, 2000).

Vasomotion and myogenic oscillations

Vasomotion is the spontaneous oscillation in tone of blood vessel walls, independent of heart beat, innervation or respiration (Haddock and Hill, 2005). It consists of rhythmic oscillations in vessel diameter and has been detected both *in vitro* and *in vivo* (Aalkjaer et al., 2011). No specific frequency is currently associated with vasomotion, and the range reported, mostly based on visual inspection in the time domain, is quite wide spanning between 0.01 and 0.5 Hz. There are several reasons. The oscillations are not clock-like, but rather quasi-periodic. For the frequency content to be resolved in detail one needs long resting-state recordings (at least 30 min, or longer), and time-frequency spectral characterisation methods. The frequency content also varies from species to species, roughly scaling with heart rate and vessel size (Bertuglia et al., 1991; Colantuoni et al., 1984b,a; Stefanovska, 2007). The smooth muscle cells, endothelial cells and the sympathetic nerves innervating the vessels, are all involved in maintaining the vascular movement and each seems to manifest itself at a different frequency (Kvandal et al., 2006).

The existence of 0.1 Hz oscillations in vessel radius have frequently been reported in humans. These oscillations correspondingly modify blood flow to produce quasi-periodic fluctuations known as flowmotion (Schmidt et al., 1992). Using the wavelet transform, 0.1 Hz oscillations have been detected in signals measured by laser Doppler flowmetry (Kvandal et al., 2003; Kvernmo et al., 1998; Söderström et al., 2003; Stefanovska et al., 1999; Stefanovska, 2007). There is still no general agreement about their origin, despite extensive discussions in the literature. Some authors attribute these oscillations to the sympathetic nervous system (Cevese et al., 2001; Stauss et al., 1998) and have associated them with baroreceptor activity that modulates the frequency of the heart thereby controlling and stabilizing blood pressure. Others have concluded that the 0.1 Hz oscillation is caused directly by the spontaneous contractions of pressure-sensitive pacemaker cells within the smooth muscles of the arterial walls (Johnson, 1991; Söderström et al., 2003), and thus that it does not originate directly from the sympathetic system.

Studies on skin-flaps and under local or general anæsthesia have further elucidated the origin of these oscillations (Söderström et al., 2003; Landsverk et al., 2006, 2007). In these cases recordings have been made while sympathetic nerves reaching the vascular myocytes were either not existing, or temporarily blocked, and spontaneous myogenic (0.1 Hz) oscillations could be distinguished from the slower purely sympathetic oscillation (0.04 Hz). In what follows, we will therefore refer to the oscillations at around 0.1 Hz as *myogenic*.

Myogenic oscillations, whether spontaneously activated due to the smooth muscle cell ionic conductances, or stimulated by a sympathetic inflow, contribute to the regulation of vascular stiffness, which is of crucial importance in hypertension. Hence, their evaluation *in vivo* could help indicate the efficacy of different treatments.

2 METHODS

2.1 Subjects

Three groups of subjects were investigated: 29 young healthy subjects (group Y, aged 24.4±3.4 years); 22 aged healthy subjects (group A, aged 71.1±6.6 years); and 22 aged treated hypertensives (group ATH, aged 70.3±6.7 years). General data for all three groups of subjects are summarised in Table 2 including their

Group	N	Age (y)	Min/Max (y)	SBP (mmHg)
Y	29 (14F)	24.4 ±3.4	18/29	118.2 ± 16.2
A	22 (13F)	71.1 ± 6.6	61/90	123.7 ± 12.5
ATH	22 (10F)	70.3 ± 6.7	59/84	138.8 ± 16.4

Table 2. Age and blood pressure data of the three groups

systolic blood pressure (SBP). All subjects except ATH had SBP <150 mmHg and diastolic BP <90 mmHg. All had body mass indices <30, and skin temperature during recording >28.5 C^o. Clinically relevant information about the ATH group is given in Tables 3 and 4 of the Appendix I. Informed consent was provided by all participants. The study was approved by the UK Northwest Research Ethics Committee.

2.2 Signals and preprocessing

Signals were recorded for 30 minutes, with subjects relaxed and supine at room temperature 21±1 C^o. The ECG was obtained from a bipolar precordial lead similar to the standard D2 lead. To maximise R-peak sharpness, electrodes were positioned on the right shoulder and in the fifth intercostal space in the left anterior axillary line. Respiratory effort was recorded using a belt encircling the subject's chest, fitted with a Biopac TSD201 Respiratory Effort Transducer (Biopac Systems Inc., CA, USA). Skin blood flow was measured by laser-Doppler flowmetry (LDF), using a MoorLAB blood flow monitor with an MP1-V2 probe (Moor Instruments, Axminster, UK), with a near-infrared laser diode producing an output power of 1.0 mW at a wavelength of 780 nm. In the resting state, the concentration of red blood cells can be considered constant, and so a Doppler shift in the velocity signal provides a measure of microvascular flow. In what follows we will use "blood flow" for skin blood flow recorded in this way (also referred to as SBF). A flexible probe holder with probe was attached to the skin on the inside front of the right wrist (caput ulna) by a double-sided adhesive disk. The time constant of the flow monitor was set to 0.1 s. The signals were recorded simultaneously (16-bit A/D converter, sampling frequency 400 Hz) using a signal conditioning system (Cardiosignals, Institute Jožef Stefan, Slovenia).

The LDF signals contained no more than 1% of artifacts; the ECG recordings included fewer than 50 ectopic beats in total; and the breathing rates of all subjects lay within the normal physiological parameters for the respiratory frequency band (0.145-0.6 Hz).

The LDF signals were resampled to 40 Hz, and examined visually to check for movement artifacts, which were removed by interpolation with cubic Hermite polynomials.

R-R interval time-series (i.e. of beat-to-beat intervals, the reciprocal of HRV) were obtained from the R-peaks in the ECG signal (marked events method, with linear interpolation).

2.3 Analysis

We conducted a comprehensive analysis of the cardiovascular oscillations and their interactions. In doing so, we first investigated the *existence* and *strength* of the oscillations, then we *decomposed* and *extracted* the oscillations, after which we quantified their *coordination* and *coherence* so that, in the end, we were able to reconstruct the coupling functions describing the *interaction mechanisms*. The methods used are explained succinctly below.

2.3.1 Existence and strength of the oscillations – use of the wavelet transform

The signals (examples in Fig. 2) were first analysed using the continuous wavelet transform (WT), which copes with the inherent non-stationarity and time-variability of physiological signals (Stefanovska et al., 1999). The WT also provides logarithmic frequency resolution (not achievable with a Fourier transform), thus yielding an appropriate representation of the low frequency spectral structure. Before applying the WT, signals were detrended by subtracting a 200 s moving average, and de-meaned. In this way, the frequency content was strongly attenuated below 0.005 Hz.

The continuous wavelet transform (WT) of a signal $s(t)$ was used in the form

$$WT(\omega, t) = \int_0^\infty \psi(\omega(u-t))s(u)\omega du, \tag{1}$$

where ω denotes angular frequency, t is time, and $\psi(u) = \frac{1}{2\pi}(e^{i2\pi f_0 u} - e^{\frac{(2\pi f_0)^2}{2}})e^{\frac{-u^2}{2}}$ (with i the imaginary unit, a central frequency of $f_0 = 1$, and $\int \psi(t)dt = 0$) is the complex Morlet wavelet.

The WT belongs to the family of time-frequency representations and contains both the phase and amplitude dynamics of the oscillatory components in the signal. With the normalizations of (1), the value of $|W_s(t, f)|^2$, often called the normalized scalogram, can be regarded as the instantaneous power spectral estimate at each time t. We therefore refer to $|W_s(t, f)|^2$ as the wavelet power, so that e.g. if one has $s(t) = A\cos(2\pi t)$ it will, at all times, have a peak of height A^2 located at $f = 1$ Hz. The time-averaged wavelet power is quite similar to the usual power spectrum (estimated from the Fourier transform after smoothing in frequency or time). However, in the latter case the smoothing is performed with a constant window, leading to spectral resolution of the oscillations on the basis of their frequency difference, i.e. linear frequency resolution. Thus e.g. the spectral resolution between oscillations with periods of 10 and 100 s (0.1 and 0.01 Hz) will be almost the same as of that of oscillations with periods 10 s and 5 s (0.1 and 0.2 Hz). In contrast, the WT has an adaptive window leading to logarithmic frequency resolution, distinguishing frequency components on the basis of the ratio of their frequencies (or periods), and thus yielding good resolution of the low-frequency spectrum.

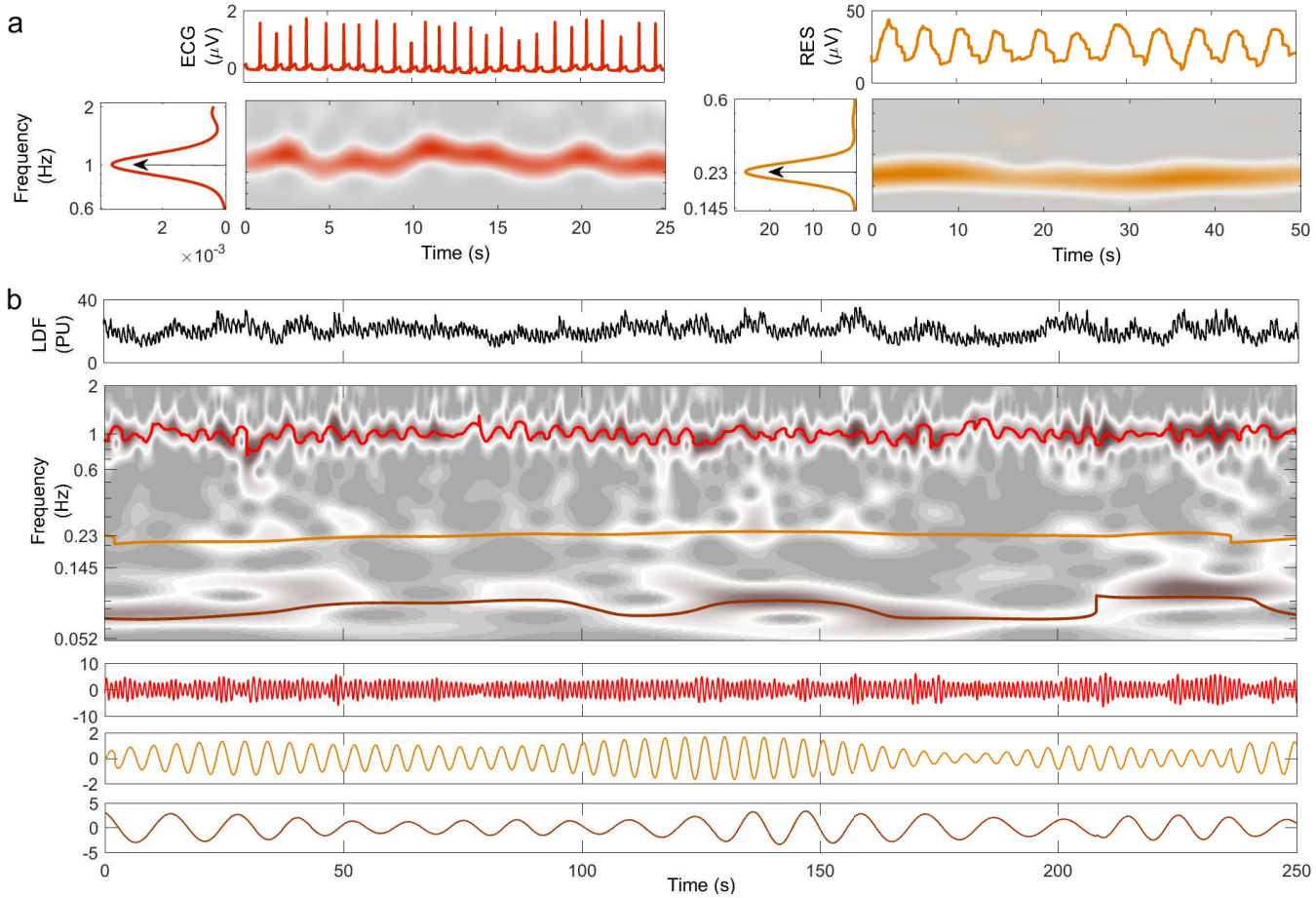

Figure 2. Decomposition into oscillatory modes: (a) Typical time windows of the signals, their wavelet transforms, and their averaged power spectra. The central frequency of each oscillation is shown for ECG (red) and respiration (orange). (b) A 250-second window of the LDF signal from the same subject is shown in the top panel. The time-frequency evolutions of the modes extracted by NMD (second panel) are indicated by colour with heart-rate red, respiration orange, and myogenic brown. The time evolutions of the extracted modes are plotted below, with the same colour-code.

Two typical windows of RES and ECG signals from a young subject are shown at the top of Fig. 2(a). The WT of each signal within the investigated frequency band is shown below its time series: a ridge corresponding to the characteristic frequencies of cardiac (left) and respiratory (right) activity clearly emerges in the time-frequency plane. The central frequency characterising each subject's cardiac and respiration rhythms is then determined by the peak value of the time-averaged spectral information, shown by the arrows on the side panels of Fig. 2(a).

2.3.2 Decomposition and extraction of oscillations – the use of nonlinear mode decomposition

The recently-introduced method of nonlinear mode decomposition (NMD) (Iatsenko et al., 2015) enables extraction of a time-variable oscillation by following the sequence of corresponding ridges in the wavelet transform plane (Iatsenko et al., 2016) and isolating the noise. Features of the method and related procedures used here include:

- The possibility of focusing the investigation of each mode on the appropriate section of the spectrum, i.e. on the subject-dependent central frequency detected by the WT.
- The use of ECG and RES time series as references for extracting cardiac and respiration oscillations from the LDF signals.
- The sequential subtraction of each decomposed mode from the original signal, before extracting the next one. This procedure excluded overlapping between the oscillations, thus enhancing the dynamical Bayesian inference (see below).

Fig. 2(b) shows the results of NMD applied to the LDF signal from the same young subject as in part (a). The LDF time series is shown on the top in Fig. 2(b), and the corresponding WT is shown below it in grey-scale. The frequency evolution in time of the extracted modes is superimposed in colour on the WT: red is used for cardiac, orange for respiration and brown for myogenic. Note that the coloured lines follow the trend of the grey ridges and are centred around the frequencies determined in Fig. 2(a). The time series corresponding to the modes are illustrated in the three panels below the WT in Fig. 2(b), following the same colour code as before. Both frequency and amplitude modulation, consistent with the WT ridges, are evident in this representation.

2.3.3 Coordination of oscillations – the use of wavelet phase coherence

Frequency-resolved phase coherence is a useful technique for studying the phase relations and coordination of the oscillations (Bandrivskyy et al., 2004; Mormann et al., 2000; Sheppard et al., 2012; Xie et al., 2017). The phase coherence between the two signals $s_{1,2}(t)$ is determined through their WTs as

$$WPC(f) = \sqrt{\langle \sin(\Delta_\phi(f)) \rangle^2 + \langle \cos(\Delta_\phi(f)) \rangle^2}, \tag{2}$$

with $\Delta_\phi(f)$ equal to the difference of the WT angles of $s_1(t)$ and $s_2(t)$ at the frequency f and all times. It reflects the extent to which the phases (and thus the underlying activities) of these signals at frequency f are correlated. Unlike the usual coherence measures, wavelet phase coherence takes no account of the amplitude dynamics of the signals. This is appropriate because the relationships between the amplitudes of common physiological oscillations in different signals can be complicated and nonlinear, but in all cases the relationship between their phases remains the same (up to the constant phase shift).

Time-localized coherence. To reveal the evolution of coherence in time, one can calculate it in a sliding window, in which case it is called time-localized coherence (Sheppard et al., 2012). To establish the appropriate amount of information for a reliable coherence measure at each frequency, we use adaptive windows of time length nc/f, which thus contain the chosen number of nc cycles at each frequency. We use $nc = 50$ for the time-localised coherence presented in Fig. 5(c).

2.3.4 Interaction mechanisms – coupling functions through the use of Bayesian inference

Modelling the data with coupled phase oscillators (Kuramoto, 1984), we apply dynamical Bayesian inference (DBI) to extract the optimal set of parameters describing the model. The method is capable of isolating the noise, and following the time-varying behaviour typical of living systems (Duggento et al., 2008; Stankovski et al., 2012; Wilting and Lehnertz, 2015). By decomposing the system into a set of interacting phase oscillators, it is possible to isolate the specific influence of each oscillator on the others, in order to generate the observed behaviour of the system, i.e. the effective coupling (Kralemann et al., 2013; Stankovski et al., 2014a).

The dynamical mechanism of interaction between a pair of oscillators can be described visually by the form of the corresponding coupling function (Kralemann et al., 2011; Stankovski et al., 2012, 2015, 2017a). To facilitate comparisons between coupling functions, two quantities have been calculated: (i) the *coupling strength* (σ) (7), based on the Euclidean norm of the coupling coefficients (Kralemann et al., 2013; Stankovski et al., 2015); and (ii) the *maximal polar similarity* (ρ) (Stankovski et al., 2017b) (9). The latter index, introduced here, is based on bi-dimensional correlation, and can thus capture specific features of the coupling functions by quantifying their morphological similarities (Kralemann et al., 2013; Stankovski et al., 2015) and phase shift.

Numerous methods exist for the inference of interactions between oscillators (Bahraminasab et al., 2008; Jamšek et al., 2010; Jirsa and Müller, 2013; Paluš and Stefanovska, 2003; Rosenblum and Pikovsky, 2001; Varela et al., 2001). Among them, dynamical Bayesian inference (DBI) (Smelyanskiy et al., 2005; Stankovski et al., 2012; von Toussaint, 2011) has the power to provide information, not only about the presence of an interaction, but also about its underlying mechanisms. In this mathematical context, *mechanism* is defined by the functional form which specifies the rule and process through which the input values are translated into output values, i.e. for a particular system it prescribes how the input influence from a second system gets translated into consequences in the output of the first system.

To tackle the inverse problem of determining coupling connections from a measured signal, the system is modelled as a network of N coupled phase oscillators (Kuramoto, 1984; Pikovsky et al., 2001). The system of N stochastic differential equations subject to noise has time-varying parameters, and it is defined as:

$$\dot{\phi}_i(t) = \omega_i(t) + q_i(\phi_i, \phi_j, \phi_k, \ldots, \phi_N, t) + \xi_i(t) \tag{3}$$

with $i = 1, \ldots, N$, where the instantaneous frequency $\dot{\phi}_i$ of each oscillator is determined by the combination of its natural frequency ω_i and a function q_i of all the N oscillators' phases $\phi_{1,\ldots,N}$ representing the coupling configuration. The stochastic part is modelled by the Gaussian white noise ξ_i. The deterministic periodic part of (3) can be Fourier-decomposed into a sum of base functions $\Phi_k = \exp[\imath(k_1\phi_1 + k_2\phi_2 + \ldots + k_N\phi_N)]$ (Duggento et al., 2012; Kralemann et al., 2011), characterised by the time-varying bank of parameters $c_k^{(i)}$:

$$\dot{\phi}_i(t) = \sum_{k=-K}^{K} c_k^{(i)} \Phi_k(\phi_1, \phi_2, \ldots, \phi_n) + \xi_i(t), \tag{4}$$

where K is the order of the Fourier expansion. In this study it was set $K = 2$. Starting from the phase dynamics extracted from the time-series, the aim is to compute the set of parameters $\mathcal{M} = \{c_k^{(i)}, D_{r,s}\}$ which completely describes the couplings ($c_k^{(i)}$) and the noise ($D_{r,s}$).

Bayes' theorem (Bayes, 1763) allows one to obtain the *posterior* density $p_{\mathcal{X}}(\mathcal{M}|\mathcal{X})$ of the unknown matrix of parameters $\mathcal{M}$ from $\mathcal{X}$, given a *prior* density $p_{\text{prior}}(\mathcal{M})$ (based on observations and representing previous knowledge of the unknown parameters), by building a *likelihood* function $\ell(\mathcal{X}|\mathcal{M})$:

$$p_{\mathcal{X}}(\mathcal{M}|\mathcal{X}) = \frac{\ell(\mathcal{X}|\mathcal{M})\, p_{\text{prior}}(\mathcal{M})}{\int \ell(\mathcal{X}|\mathcal{M})\, p_{\text{prior}}(\mathcal{M}) d\mathcal{M}}.$$

The likelihood function is computed through the stochastic integral of the noise term over time, leading to the minus log-likelihood function $S = -\ln \ell(\mathcal{X}|\mathcal{M})$ expressed as:

$$\begin{aligned} S = \frac{L}{2}\ln|\mathbf{D}| + \frac{h}{2}\sum_{l=0}^{L-1}\Big(\mathbf{c}_k\frac{\partial\mathbf{\Phi}_k(\phi_{\cdot,l})}{\partial\phi} + \\ + [\dot{\phi}_l - \mathbf{c}_k\mathbf{\Phi}_k(\phi^*_{\cdot,l})]^T(\mathbf{D}^{-1})[\dot{\phi}_l - \mathbf{c}_k\mathbf{\Phi}_k(\phi^*_{\cdot,l})]\Big), \end{aligned} \tag{5}$$

where summation over the repeated indices k is implicit, and the dot index in $\phi_{\cdot}$ is substituted with the relevant index.

Assuming that the prior probability of parameters $\mathcal{M}$ is a multivariate normal distribution, and taking into account the quadratic form of the log-likelihood (5), the posterior probability will also be a multivariate normal distribution. This particular distribution for the parameters $\mathbf{c}$, with mean $\bar{\mathbf{c}}$, and covariance matrix $\mathbf{\Sigma}_{\text{prior}} \equiv \mathbf{\Xi}^{-1}{}_{\text{prior}}$, can be used to calculate recursively the stationary point of S only with the following four equations:

$$\begin{aligned} \mathbf{D} &= \frac{h}{L}\left(\dot{\phi}_l - \mathbf{c}_k\mathbf{\Phi}_k(\phi^*_{\cdot,l})\right)^T\left(\dot{\phi}_l - \mathbf{c}_k\mathbf{\Phi}_k(\phi^*_{\cdot,l})\right), \\ \mathbf{r}_w &= (\mathbf{\Xi}_{\text{prior}})_{kw}\,\mathbf{c}_w + h\,\mathbf{\Phi}_k(\phi^*_{\cdot,l})\,(\mathbf{D}^{-1})\,\dot{\phi}_l + \\ &\quad - \frac{h}{2}\frac{\partial\mathbf{\Phi}_k(\phi_{\cdot,l})}{\partial\phi}, \\ \mathbf{\Xi}_{kw} &= (\mathbf{\Xi}_{\text{prior}})_{kw} + h\,\mathbf{\Phi}_k(\phi^*_{\cdot,l})\,(\mathbf{D}^{-1})\,\mathbf{\Phi}_w(\phi^*_{\cdot,l}), \\ \mathbf{c}_k &= (\mathbf{\Xi}^{-1})_{kw}\,\mathbf{r}_w, \end{aligned} \tag{6}$$

where the summations over $l = 1, \ldots, L$, and over the repeated indices k and w, is implicit. This inference technique is applied to the information provided by a stream of sequential blocks coming from the time-series and a special procedure is used for inferring time-varying dynamics. A tutorial about the practical implementation of dynamical Bayesian inference, including programming and software codes, is available (NBP-Lancaster, 2016; Stankovski et al., 2014b).

Coupling strength: The strength $\sigma_{i,j}$ of the coupling from the oscillator i to j is defined as the Euclidean norm of the inferred parameters from the phase dynamics:

$$\sigma_{i,j} = \sqrt{\sum_{k=-K}^{K}(c_k^{(i:j)})^2}, \tag{7}$$

where the parameters are defined as in Eq. (4). It gives an overall estimate of the amount of influence that the phase of the oscillator i exerts on the frequency of the oscillator j.

Polar similarity: By calculating the correlation between coupling functions, one can quantify their similarity (Kralemann et al., 2013). Here we extend this concept, by computing the correlation of a coupling function q with a bank of numerically generated forms Q having specific shape features, in order to determine which

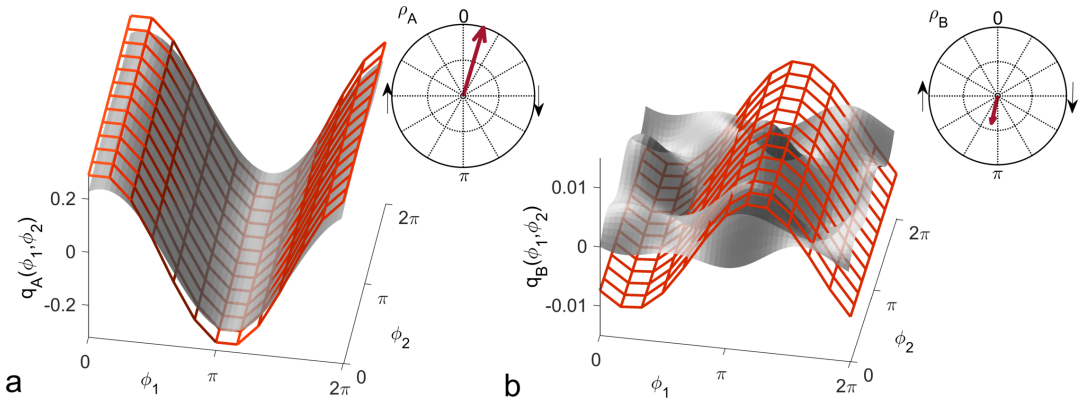

Figure 3. Examples of the similarity index for (a) high and (b) low similarity. The form obtained numerically from a unidirectionally coupled system, shown with a red grid, is shifted along the coupling function obtained from measured data, shown in gray, to detect the highest similarity modulus $|\bar{\rho}|$. The arrow in the polar plot has a modulus equal to $|\bar{\rho}|$ and a phase $\langle\bar{\rho}\rangle$ corresponding to the phase-shift of the red grid.

of those features is predominant in q. The similarity modulus is defined as

$$|\rho_q| = \frac{\langle \tilde{q}\, \tilde{Q}_\theta \rangle}{|\tilde{q}|\, |\tilde{Q}_\theta|} \times 100, \tag{8}$$

where the angular brackets denote averaging over the $2\pi \times 2\pi$ phase grid and the tilde $\tilde{}$ denotes the deviation from the mean. Values of $|\rho|$ range from 0 to 100 and are expressed as percentages. We generate coupling functions numerically with a shape which results from a unidirectional direct coupling of the slower oscillator to the faster, phase-shifted by an angle θ along the ϕ_1 axis. Thus, the numerical form Q_θ generating the highest $|\rho|$ carries dual information: the extent of the similarity (described by $|\rho|$ itself) and the corresponding phase-shift angle θ generating it, denoted by $\langle\rho\rangle$. A natural way to represent this information is by indicating it on the complex plane by the *maximal polar similarity index*, defined as:

$$\rho_q = |\rho_q| e^{i\langle\rho_q\rangle}, \tag{9}$$

where i is the imaginary unit.

The meaning of this parameter is illustrated by the two examples in Fig. 3, where the grey forms have been selected for generating very high and very low similarity indices, respectively. The superimposed red grid shows the most similar numerical form detected by the method. The arrows in the polar plots correspond to the polar similarity indices: the moduli of the arrows quantify the degree of overlap, while the angle indicates the phase of the positive maximum in the numerically generated function.

2.4 Statistical analysis and surrogates

An unpaired two-sided Wilcoxon rank sum test was used for comparisons between groups, and statistical significance was set at $p < 0.05$.

Because the phase coherence will generally be non-zero, even for completely unrelated oscillations, one needs to fix a threshold (significance level) above which coherence can be regarded as indicating genuine interdependence. For standard spectral coherence it is often set to 0.5, but such a threshold does not take into account the possibility of bias. We use the more reliable and accurate approach of applying a surrogate

test. At each frequency we estimate the coherence threshold as being 95% of the highest value of the 300 coherences calculated between R-R intervals and skin blood flow taken from different subjects. Such signals are by definition completely independent, thus providing reliable estimates that take account of possible computational or methodological bias. Generally one is interested only in coherence above the threshold, so we consider an effective coherence defined as the actual coherence minus the calculated coherence significance level.

Inter-subject surrogate analysis (Toledo et al., 2002; Iatsenko et al., 2013) was also used to validate the results for coupling functions. The same central and peripheral networks were built for 200 combinations of randomly chosen inter-group subjects (i.e. cardiac from subject A, respiration from subject B, myogenic from subject C). Each such combination is therefore composed of mutually independent signals, but preserves the statistical characteristics of the original networks. This technique allows us to identify the significance of the results by comparison with the randomly created outputs, excluding from consideration as irrelevant any result that is lower than would be given by chance or which might arise through bias.

3 RESULTS

3.1 Spectral power

3.1.1 Spectral power in R–R fluctuations

Fluctuations in R-R intervals at all frequencies decline markedly with age (not shown), in agreement with earlier work (Agelink et al., 2001; Antelmi et al., 2004; Shiogai et al., 2010). No statistically significant difference between the A and ATH groups was noticed, although the spectral power below 0.1 Hz tended to be lower for ATH.

3.1.2 Spectral power in blood flow

Very slow ($<$0.02 Hz), respiratory and cardiac oscillations in blood flow increase significantly with age (Fig. 4(a)). While there is almost no difference in blood flow spectral power below 0.5 Hz between the A and ATH groups, there is a striking difference between them in the cardiac frequency range, showing that cardiac pulses in the ATH group are weaker than in the A group.

The box-plots in Fig. 4(b) compare the power spectral content within the bands investigated for different groups: Y group is represented in gold, A in brown, and ATH in red. Group A was found to have strikingly stronger LDF cardiac oscillations than either the Y or ATH groups (p-value$<$0.001). These oscillations carry most of the total power. For the respiration band, values of the power are less widely-separated, yet are significantly lower in the Y group (p-value$<$0.05). A similar pattern was found within the myogenic band, with statistically significant differences only for the Y-ATH comparison.

3.2 Coherence between fluctuations in R-R variability and blood flow

The results plotted in Fig. 5(b) show that there is significant coherence (i.e. above the significance threshold) between skin blood flow and RR intervals in both the respiratory and myogenic intervals. However, only within the myogenic interval does the coherence differ between the groups, declining with age and nearly disappearing in treated hypertension. Fig. 5(c) presents typical examples of time-localized coherence between R-R intervals and blood flow (Sheppard et al., 2012). It not only shows that the coherence can be stable in time, but also illustrates the decrease of coherence with age and its virtual disappearance in the ATH group. In particular, 28/29 Y and 18/22 A subjects, but only 11/22 ATH subjects, had significant coherence in myogenic interval. There were no significant gender differences in the effective

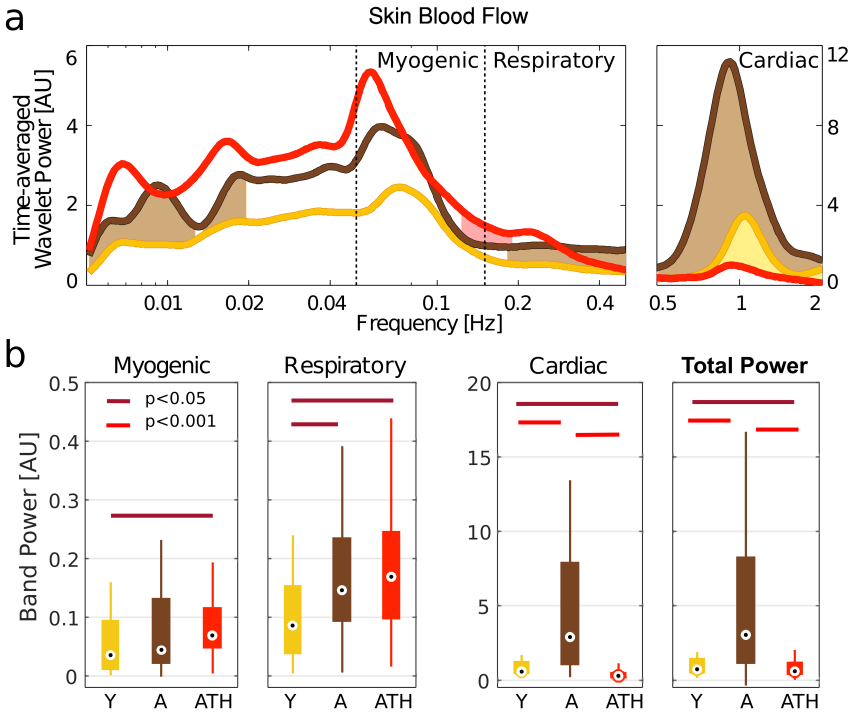

Figure 4. Wavelet power: (a) Time-averaged wavelet power of blood flow, means over groups. Brown shading indicates significance between A and Y, red shading between ATH and A, and yellow shading between Y and ATH. (b) Box-plots showing the cardiac, respiration and myogenic oscillations and the total power in the LDF signal within these three intervals. The Y group is represented in gold, A in brown, and ATH in red.

coherence within each group (not shown). Average wavelet coherence for each of the three groups is shown in the Appendix II, figure 11(c) and (d). The coherence between R-R interval time series and the finger pulse plethismography (PPG) signal is also discussed in Appendix II and shown in figures 11(a) and (b). The (PPG) signal provides a measure of changes in arterial volume proportional to changes in arterial blood pressure.

3.3 Coupling functions

Figs. 6 and 7 show the group-averaged forms of coupling for the Y (a,e), A (b,f), ATH subjects (c,g) and surrogates (d,h). In each case, the first row shows the coupling detected from the centrally extracted modes, while the second row shows the results from the peripheral network. The polar graph in the top-right corner of each plot indicates the polar similarity index ρ for each subject (thin arrows in grey) and $\bar{\rho}$ for the inter-subject average (thick coloured arrow). Values of the median similarity modulus $|\bar{\rho}|$ and strength σ for each group are listed in Fig. 8(a). The group distribution of similarity $|\bar{\rho}|$ is shown by the box-plots in Fig. 8(b) to (e). The lines over the boxes indicate the statistically significant comparisons between each pair of groups ($p<0.05$ in dark red and $p<0.001$ in bright red).

Respiration-to-cardiac coupling functions

The coupling from respiration to the cardiac rhythm, considered to be responsible for respiratory sinus arrhythmia (RSA), has been investigated both centrally and when propagated in the blood flow.

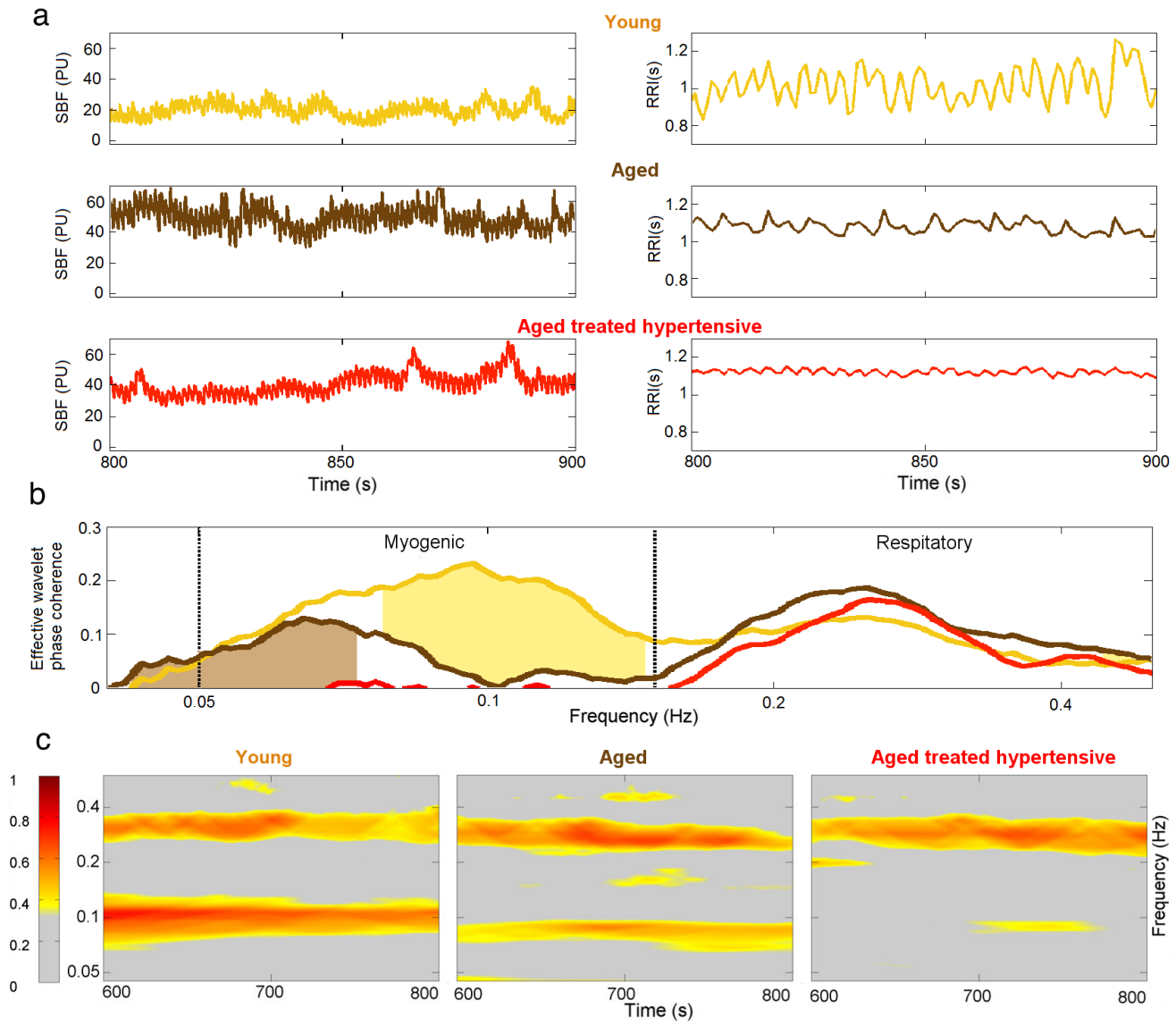

Figure 5. Phase coherence: (a) Typical SBF and R-R interval (RRI) signals from each group of subjects. PU – perfusion units; (b) Wavelet phase coherence (minus surrogate thresholds) between R-R intervals and SBF, mean over groups, where gold shading indicates significant difference between the Y and A groups and brown shading – between the A and ATH groups; (c) Time-localized wavelet phase coherence for individuals typical of the three subject groups. Note how the coherence within the myogenic interval is diminished almost to vanishing point in the ATH group.

Central network: For Y subjects, the coupling function is roughly sinusoidal. The golden arrow $\bar{\rho}_{R,C}$ in the polar plot has close-to-100% modulus and its phase is approximately $\pi/2$: it can be seen from analysis of the distribution of the grey arrows that the whole group exhibits similarly shifted forms of coupling. For A and ATH subjects, the shapes and phases of the average forms shown in Figs. 6(b) and (c) are similar: they resemble what has been discussed for Y subjects, but with smaller $|\bar{\rho}_{R,C}|$ and a larger number of phase-outliers. Fig. 6(d) shows the results for surrogates. It can be seen that the amplitude of the coupling for surrogates is negligible when compared to the real cases, and that the phases of surrogates $\langle \rho_{R,C} \rangle$ are scattered around the 2π plane with very variable $|\rho_{R,C}|$, resulting in a significantly smaller $|\bar{\rho}_{R,C}|$.

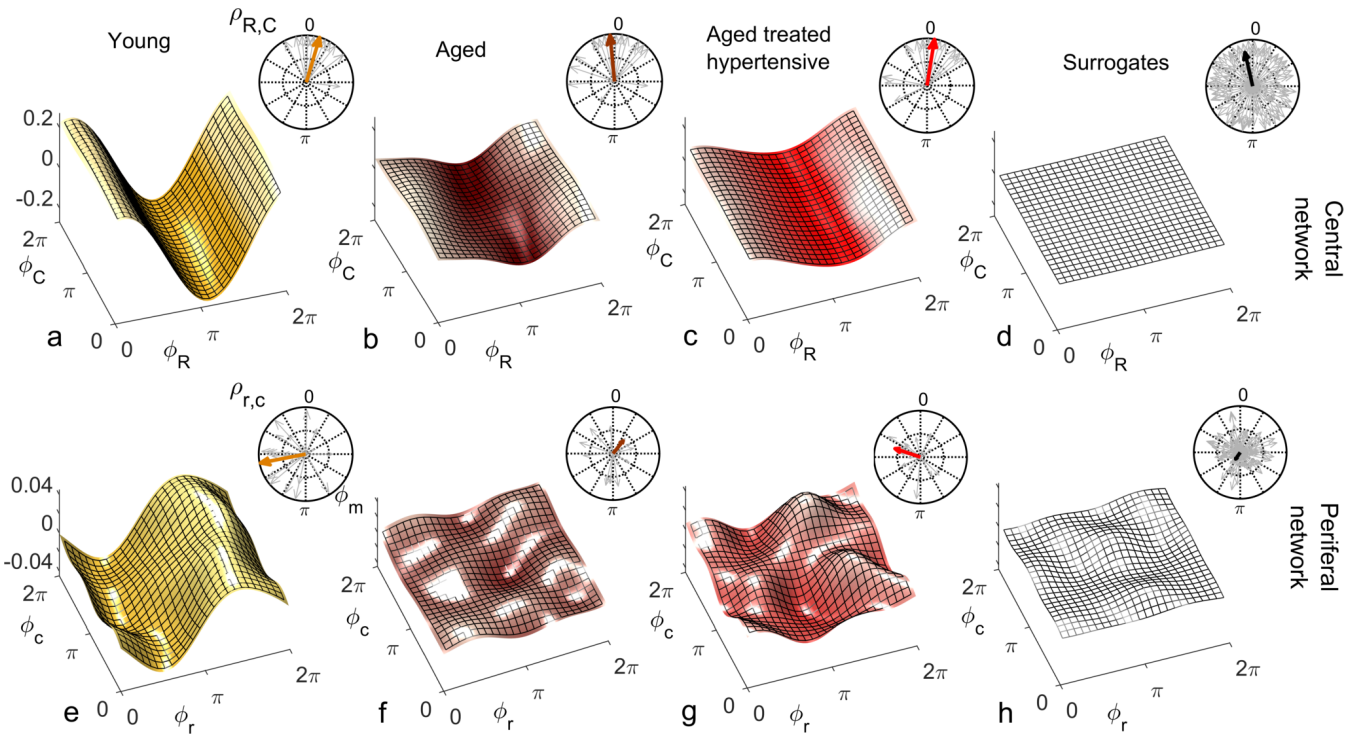

Figure 6. Group-averaged coupling functions in the central network (top row) compared with equivalent results from the peripheral network (bottom row). In each case the colour coding is: Y (gold), A (brown), ATH (red) and surrogates (grey). Panels a,b,c show the coupling functions $q_C^{R,C}$ between the phases of centrally measured respiratory ϕ_R and cardiac ϕ_C oscillations, and e,f,g show the equivalent quantity $q_c^{r,c}$ between the phase of respiratory ϕ_r and cardiac ϕ_c oscillations in the peripheral network. Plots d and h show the surrogate coupling functions computed to check the validity of the results presented in each row. The polar plot in the top-right corner of each figure indicates the similarity index ρ for the average form (coloured arrow) and for the individual subjects (grey arrows). Note how, with ageing, the forms lose amplitude in the central network and resemble the variability of surrogates in the peripheral network.

The median values of $\sigma_{R,C}$ are given in Fig. 8(a). In the case of the central network, the strength of the direct coupling exerted on the cardiac component by the respiratory mode differs significantly from that of the corresponding surrogates, for all groups ($p<10^{-8}$). For Y subjects, $\sigma_{R,C}$ differs significantly from that of the other groups ($p<10^{-6}$), while the A and ATH subjects show overlapping medians ($p>0.6$). The same significance pattern appears in the similarity box-plots of Fig. 8(b): only the comparison between A and ATH groups is not significant. For the similarity, the distribution of surrogates is spread along the 0-100% axes of $|\rho_{R,C}|$, with a median value around 70%, while the distributions computed for all three Y, A, ATH groups, are all narrowly grouped around median values lying above 95%.

Peripheral network: Fig. 6(e) shows that the form of coupling discussed for $q_C^{R,C}$ is still detectable in $q_c^{r,c}$ for the Y group even if with considerably smaller amplitude. The forms of coupling for the A group (Fig. 6(f)) and ATH (Fig. 6(g)) subjects are similar to that obtained from the surrogate data (Fig. 6(h)). The polar plots of Fig. 6(f) and (g) show that the A group and ATH subjects are characterized by lower moduli of similarity $|\rho_{r,c}|$, with phase shifts $\langle\rho_{r,c}\rangle$ scattered all around 2π. The similarity boxplots in Fig. 8(c) show that $|\rho_{r,c}|$ for the Y subjects is significantly higher ($p < 0.05$) than that for the three other groups (including the "surrogate group"), and that there are no significant differences between those three groups. The coupling strength $\sigma_{r,c}$ for the A and ATH groups does not differ significantly from that obtained from surrogate data. The only significance found was between Y group and surrogate data (see Fig. 8(a)).

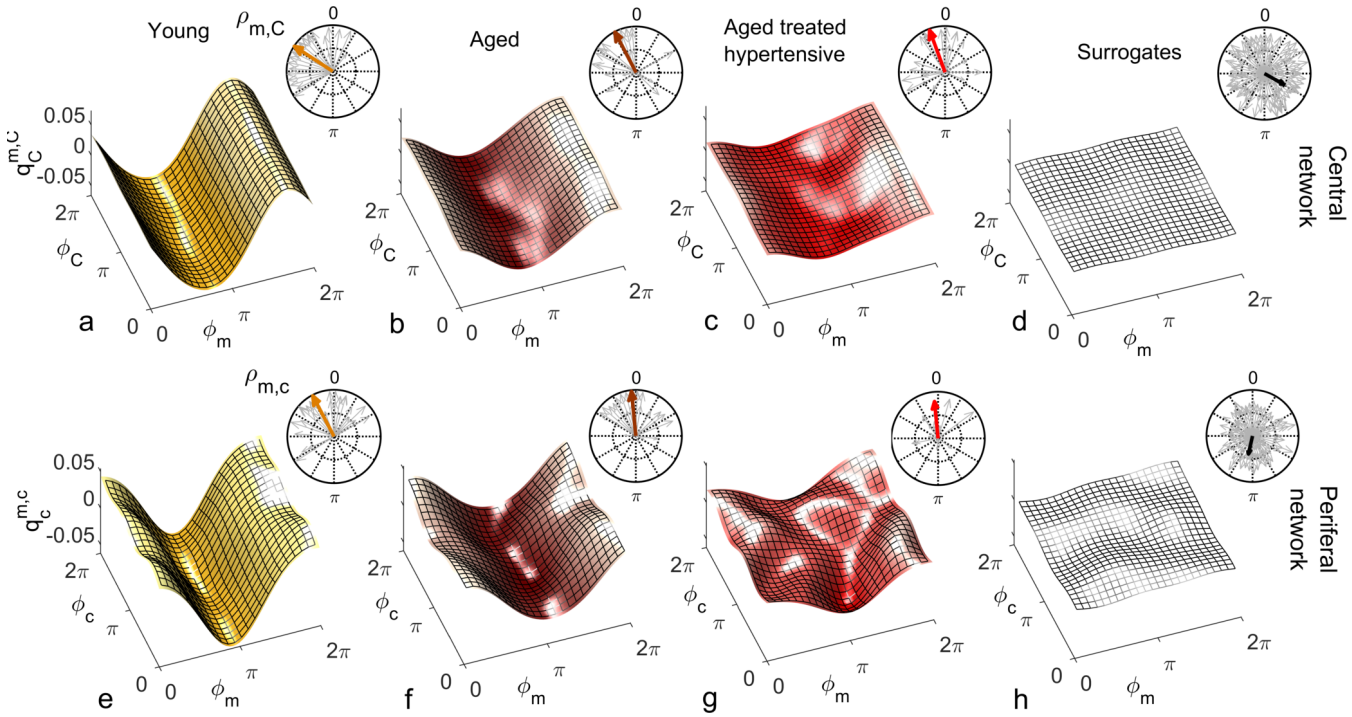

Figure 7. As in Fig. 6 except that a,b,c represent the coupling functions $q_C^{m,C}$ between the phase of myogenic ϕ_m and cardiac ϕ_C oscillations in the central network and e,f,g show $q_c^{m,c}$ between the phases of myogenic ϕ_m and cardiac ϕ_c oscillations in the peripheral network. Plots d and h are from the corresponding surrogates. Again, the forms lose amplitude with ageing in the central network, and with hypertension, resemble the variability of surrogates in the peripheral network.

Myogenic-to-cardiac coupling functions

The coupling between myogenic and cardiac oscillations was also investigated both centrally and when propagated in the blood flow. The phase of the myogenic oscillations extracted from LDF was used in both cases, while the phase of the cardiac oscillations was extracted from ECG or LDF respectively.

Central network: The forms of coupling function in the first row of Fig. 7 follow the same trend as the cardio-respiratory ones: in each group – except for the surrogates – a sinusoidal wave clearly propagates along the ϕ_C axes. The amplitude of the averaged forms decreases from Fig. 7(a) to Fig. 7(b), and from Fig. 7(b) to Fig. 7(c). The polar plots show that the number of subjects with smaller $|\rho_{m,C}|$ and scattered $\langle\rho_{m,C}\rangle$ increases with age and especially with hypertension. The values of $|\bar{\rho}_{m,C}|$ obtained from surrogate data shown in Fig. 7(d) are comparatively small, and $\langle\rho_{m,C}\rangle$ is randomly 2π-scattered. The values of $\sigma_{m,C}$ in Fig. 8(a), for both the A and ATH subjects are indistinguishable from those for surrogate data. However, $\sigma_{m,C}$ for the Y group it is significantly higher than that for each of the other three groups ($p<0.05$). In contrast, the similarity of forms $|\rho_{m,C}|$ clearly distinguishes between the ATH and A groups. Again, the box-plots shown in Fig. 8(d) summarise the results: it is evident that the values for Y and A subjects do not differ, while values for ATH subjects do not differ significantly from those obtained from surrogate data.

Peripheral network: Fig. 7(e) is qualitatively very similar to Fig. 7(a), but with a small relative phase-shift between $\langle\bar{\rho}_{m,C}\rangle$ and $\langle\bar{\rho}_{m,c}\rangle$. The statistical analysis for $\sigma_{m,c}$ and for $|\rho_{m,c}|$ follows the same trend detected from the central network. The polar plot in the Fig. 7(f) shows that the phases $\langle\rho_{m,c}\rangle$ are clustered around a $\langle\bar{\rho}_{m,c}\rangle$ very close to $\langle\bar{\rho}_{m,C}\rangle$: from this plot and from the golden boxes in Fig. 8(e), it can be seen that most of the subjects from the A group preserve a considerable $|\rho_{m,c}|$ that is not statistically different from

a

Coupling parameters		Y	A	ATH	Surr.
$\sigma_{R,C}$	(Hz)	0.24	0.09	0.09	0.03
$\sigma_{r,c}$	(Hz)	0.07	0.02	0.05	0.04
$\sigma_{m,C}$	(Hz)	0.10	0.05	0.04	0.06
$\sigma_{m,c}$	(Hz)	0.11	0.06	0.07	0.07
$\lvert\rho_{R,C}\rvert$	(%)	99.5	98.4	98.8	73.7
$\lvert\rho_{r,c}\rvert$	(%)	59.2	42.3	39.4	29.8
$\lvert\rho_{m,C}\rvert$	(%)	95.5	94.7	79.6	65.9
$\lvert\rho_{m,c}\rvert$	(%)	86.5	86.5	31.2	43.3

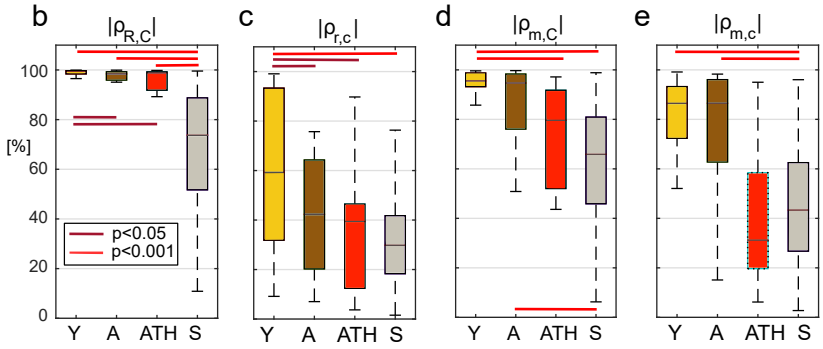

Figure 8. Statistics for coupling parameters. (a) Table showing the median values for the coupling strength σ and modulus of similarity $|\rho|$ for groups of Y, A, ATH subjects and surrogates, with median values not significantly different from surrogates are shown in grey. Box-plots picturing the distributions of the similarity modulus $|\rho|$ within each group, using the same colour map as Fig. 4. The relation between respiration and cardiac for the (b) central and (c) peripheral networks and of myogenic and cardiac for the (d) central and (e) peripheral networks.

the Y group's distribution. For hypertension (Fig. 7(g)), the average form of the coupling shown in Fig. 7(f) is more ragged. The phases $\langle\rho_{m,c}\rangle$ are scattered in the 2π plane, and the coupling between ϕ_m and ϕ_c generates forms with small $|\rho_{m,c}|$. The boxes of Fig. 8(e) summarise the results, indicating no difference in $|\rho_{m,c}|$ between Y and A groups, while values for the ATH group are indistinguishable from those obtained from surrogate data.

4 DISCUSSION

By analysis of phase coherence and coupling functions we have been able to study how cardiovascular and microvascular dynamical processes change with ageing and hypertension using only resting-state recordings, without any need to stimulate or perturb the system.

The significant increase in very slow (≤ 0.02 Hz), respiratory and cardiac oscillations in blood flow with age (Fig. 4) could be explained by results obtained in earlier studies which showed that small arterioles are dilated in the elderly (Kelly et al., 1995) and that the diameter of the larger arteries increases together with a decrease in elasticity (Levy, 2001). Hence, the increased vessel radii and decreased vessel elasticity may have resulted in larger oscillations. The striking difference between the A and ATH groups' time-averaged wavelet power in the cardiac frequency range shows that cardiac pulses in the ATH group are not restored to age matched normal. This suggests an increased stiffness of arterioles in ATH patients, a defect that persists despite antihypertensive therapy.

The reduction in 0.1 Hz interval coherence seen in the ATH group (Fig. 5) indicates an additional cardiovascular system abnormality that is not restored by antihypertensive treatment to age matched normal. The results appear to imply a progressive impairment with age of the underlying mechanisms of coordination between cardiac and vascular activity, and with even greater impairment in hypertension.

The lack of significant 0.1 Hz interval coherence between R-R and SBF in the ATH group suggests local changes of the skin microvasculature, an inference that is supported by an additional finding: a loss of significant 0.1 Hz interval coherence between blood flow measured on different sites (not shown). This may perhaps be an indication of impaired myogenic activity observed via the blood flow signal. This explanation is consistent with the reported increase of stiffness and basic myogenic tone in the arteries of hypertensive patients (Feihl et al., 2006; Yannoutsos et al., 2014), which may also explain the decrease in

the amplitude of cardiac oscillations in the blood flow of the ATH group (Fig. 4). This abnormality is not restored to aged matched normal by treatment.

Coupling functions provide additional insight into the changes that occur with ageing and hypertension. For the central network, the mechanism of RSA is captured by the coupling functions. The sinusoidally-shaped wave propagating along the respiration phase axes ϕ_R in Fig. 6(a) indicates that the coupling between ϕ_R and ϕ_C with the cardiac rhythm depends on the phase ϕ_R: namely, the heart rate accelerates on the second part of the respiratory cycle i.e. after inhaling ($q_C^{R,C}<0$), and decelerates during the initial part of the cycle, i.e. after exhaling ($q_C^{R,C}>0$). These results are consistent with earlier work (Iatsenko et al., 2013; Kralemann et al., 2013). Furthermore, the polar plots give additional insight into the group dynamics. The comparison between groups in Fig. 6(a) to (c) suggests that RSA weakens but is nonetheless preserved in aged subjects. Treatment for hypertension does not seem to influence this phenomenon.

For the peripheral network, the difference in coupling between respiratory and cardiac waves between the groups of young and aged subjects becomes more evident. Within this network, the phase shift displayed by the form of coupling for young subjects (Fig. 6(a) and (e)) reflects the time-delay that the respiration wave undergoes during its propagation to the peripheral vascular network, Because the distribution of $|\rho_{r,c}|$ for the aged groups is not significantly different from that of the surrogates, we conclude that the interaction between the phases ϕ_r and ϕ_c in the vascular bed weakens with ageing. This result is not dependent on the propagation of the waves themselves: the investigation of spectral power shown in Fig. 4 revealed that both the respiratory and cardiac oscillations are stronger in healthy aged subjects than in the young group ($p<0.05$). Ageing-related loss of tone in the walls of big vessels is thought to play a role by offering less resistance to blood-flow and therefore easing the propagation of centrally-generated waves (Levy, 2001).

The most interesting outcomes of the study are related to the myogenic oscillation. The reduced coherence of the myogenic interval seen in the ATH group (Fig. 5(b) and (c)) indicates a cardiovascular system abnormality that is not restored by antihypertensive treatment. The results appear to imply a progressive impairment with age of the underlying mechanisms of coordination between cardiac and vascular activity, and with even more impairment in hypertension. Antihypertensive treatment is evidently unable to correct this defect; we found no evidence to suggest that the medications listed in Table 3 differ in efficacy in this respect. The treatments were diverse, however, and the number of subjects under exactly the same treatment regimens were too small to allow for a reliable statistical comparison.

To get deeper insight into this 'asynchrony', myogenic-to-cardiac couplings were analysed and studied here for the first time. For young subjects, the coupling strength $\sigma_{m,C}$ of the central network is significantly higher than that for the other groups. This result indicates that the myogenic activity of the skin microvessels shares functional properties with those of the cardiac muscle, and it confirms that the coupling between myogenic activity detected in microvasculature and cardiac activity fades with ageing. Box-plots in Fig. 8(d) show how both Y and A, but not the ATH group, have a similarity modulus significantly higher than surrogates.

Analysis of the peripheral network for the myogenic-cardiac interaction generated similar results. There was an even clearer difference between the moduli of similarity obtained from A and ATH subjects. Box-plots for the similarity of the forms in Fig. 8(e) cluster the subjects into two statistically distinct groups: Y with A, and ATH with surrogates.

It had already been shown that antihypertensive medication does not necessarily improve endothelial function (Ghiadoni et al., 2003). Moreover an impaired efficiency of myogenic activity within the hypertensive vascular system was also suggested by an earlier study, which did not improve with anti-hypertensive

treatment (Rossi et al., 2006). Results for the similarity modulus $|\rho|$ demonstrate that myogenic and cardiac oscillations are less strongly coupled in hypertensive than in healthy aged subjects, despite the treatment. This highlights how the comparative similarity of forms can reveal characteristics of the coupling mechanism that would remain undetected by investigations just based on coupling strength. Counter-intuitively, the myogenic spectral power (box-plots in Fig. 4) was found to be significantly higher in hypertensive than in young subjects. Similarly to what was discussed for the case of respiration, this outcome supports the theory that what is affected is not the magnitude of the oscillation, but its capacity to adjust to the dynamical interactions to which it is being subjected.

One can expand the analyses presented here, and the phases of the three oscillatory components can also be extracted from other signals, if simultaneously recorded. One such candidate is a signal providing information proportional to the blood pressure, rather than to blood flow as used in this study. For example, the signal of finger pulse photoplethysmography (PPG, see e.g. (Allen, 2007)) was simultaneously recorded in all our subjects and is therefore available together with the other signals. The changes in finger volume result from the involvement of arterioles, as well as the microvasculature, and hence the myogenic contribution comes on average from larger vessels than those recorded by the LDF. To verify whether the observed difference in coherence between the R-R intervals and the blood flow at the myogenic interval between A and ATH groups also exists when larger vessels are included, the same analysis as that presented in Fig. 5b was performed, but using the PPG signal. No statistically significant differences were observed between the two groups (see Appendix II), which can be taken to indicate that the blood pressure control mechanisms related to smooth muscle cells are probably restored by the current antihypertensive treatment. This further demonstrates that it is the endothelial involvement (Furchgott and Zawadzki, 1980) that is still impaired, as this is dominant in the microvasculature. These results are in agreement with an earlier study (Ebert et al., 1992) where, based on recordings of muscle sympathetic nerve activity (MSNA), it was shown that, although the parasympathetic component of the arterial baroreflex becomes impaired with advancing age, the sympathetic component can be well maintained in healthy individuals even into the seventh decade. The methodology presented here can thus be further used to investigate coherences and couplings from any signals recorded simultaneously from the cardiovascular system. Note, however, that special care is needed: a minimum length of recording is required; and the phase of the oscillations should be extracted with sufficient precision for the calculations to be meaningful.

A difficulty in doing research on treated hypertensive patients is the large range of different drugs, each with its own separate mode of action, that one may encounter. Indeed, as shown in Table 4, a wide variety of drugs was used to treat the subjects included in our study: their inclusion was based on the fact that their hypertensive treatment has been individually optimised for maximal success. So our study does not make it possible to find out which of the drugs are less, or more, effective. Nonetheless, in a cohort of patients with optimally treated hypertension, according to the current doctrines, we have shown that there is still residual microvascular impairment. The same methodology can clearly be used to evaluate the effect of individual drugs, or for a longer-term follow up of a treatment for hypertension, and may help in the development of new medications.

In conclusion, by investigating the deterministic properties of the HRV signal together with simultaneously recorded respiration and microvascular blood flow signals, and by extracting time-dependent parameters, we have gained insights that are clinically relevant to studies of ageing and hypertension. While cardiorespiratory couplings and interactions in general have been studied previously, here we have investigated for the first time phase coherence and coupling between myogenic activity and cardiac and respiratory oscillations. The significant impairment of coherence within the myogenic interval of the

ATH group as recorded in the microvasculature seems to imply that some of the current treatments for essential hypertension fail to restore microvascular regulation. Similarly, treated hypertensive subjects differ from the healthy control group of the same age in terms of the coupling between cardiac and myogenic oscillations within the peripheral network. Thus hypertension affects the myogenic microvascular structure by uncoupling the system of oscillators of which it is composed. It is clear that current anti-hypertensive treatments, while successfully controlling blood pressure, do not restore microvascular function.

CONFLICT OF INTEREST STATEMENT

The authors declare that the research was conducted in the absence of any commercial or financial relationships that could be construed as a potential conflict of interest.

AUTHOR CONTRIBUTIONS

V.T. completed the coupling functions analysis with advice and supervision from T.S., created figures, and drafted the manuscript. D.I. completed the phase coherence analysis, created figures, and drafted the associated text. A.B. measured and analysed data. A.E.B. helped to recruit the hypertensive patients, measured data and did preliminary analysis. A.R.G. recruited and selected the hypertensive patients. P.V.E.McC. helped to supervise the study and contributed to writing the manuscript. P.B.M.C. provided clinical support and contributed to the interpretation of the results. A.S. conceived, planned and supervised the study, and contributed to the development of the algorithms and to the writing of the manuscript. All authors discussed the results and contributed to the editing of the manuscript.

FUNDING

The work was supported by the Engineering and Physical Sciences Research Council, United Kingdom (Grant No. EP/100999X1), by the EU project COSMOS (Grant No. 642563), by the Joint Research Councils' New Dynamics of Ageing programme administered by the Economic and Social Research Council, United Kingdom (Grant No. RES-356-25-0006), by the Action Medical Research (UK) MASDA Project [GN1963], and by the Slovenian Research Agency. VT is supported by a PhD grant from the Department of Physics, Lancaster University.

ACKNOWLEDGMENTS

We acknowledge valuable discussions with Dwain Eckberg, Maja Elstad, Djordje Jakovljevic, Helena Lenasi and Angela Shore.

APPENDIX I – PARAMETERS FOR PATIENTS AND HEALTHY SUBJECTS

Parameter	Mean ± SD	Medications taken	Number of subjects
Age (years)	70.3 ± 6.7	Beta-blockers	10
Systolic pressure (mmHg)	138.8 ± 16.4	ACE inhibitors	10
Ankle brachial pressure index	1.08 ± 0.09	Angiotensin receptor blockers	4
Total cholesterol (mmol/l)	4.26 ± 1.22	Calcium channel blockers	9
HDL cholesterol (mmol/l)	1.36 ± 0.38	Diuretics	8
LDL cholesterol (mmol/l)	2.32 ± 0.99	Statins	16
Triglycerides (mmol/l)	1.31 ± 0.53	Aspirin	12
hs-CRP (mg/l)	2.62 ± 2.03		
Capillary refill time (s)	2.5 ± 0.6		
Height (m)	1.68 ± 0.10		
Weight (kg)	77.6 ± 16.5		
Body mass index (kg/m2)	27.2 ± 3.9		
Time since diagnosis (years)	10.0 ± 6.2		

Table 3. Summary of the hypertension-related parameters and of the medication being taken by the ATH group

Age	Sex	Blood Pressure (mmHg)	Years since diagnosis	RR-PPG myogenic coherence	RR-LDF myogenic coherence	Beta-blockers	ACE inhibitors	Angiotensin receptor blockers	Calcium channel blockers	Diuretics	Statins	Aspirin
70	F	NA	16	Y	Y	Y	N	N	N	N	Y	N
69	M	NA	7	Y	Y	N	Y	N	N	N	Y	Y
71	M	162	10	Y	N	Y	Y	N	N	Y	Y	Y
66	F	150	12	Y	Y	N	Y	N	N	Y	Y	Y
60	F	171*	9	Y	Y	N	N	N	N	N	N	Y
75	F	145	6	Y	N	Y	N	N	Y	Y	Y	Y
70	M	131	7	Y	N	Y	N	N	Y	N	Y	Y
79	M	120	13	Y	N	N	Y	N	N	N	N	N
74	F	145	14	Y	N	N	Y	N	N	Y	Y	Y
80	F	138	NA	Y	N	Y	N	Y	Y	N	Y	Y
68	M	115	2	Y	N	N	Y	N	N	N	Y	Y
64	M	155	8	Y	Y	Y	Y	N	N	N	Y	N
68	M	125	6	Y	N	Y	N	Y	N	N	Y	N
84	F	145	28	Y	N	Y	N	N	Y	N	Y	N
59	M	125	6	Y	N	N	N	Y	N	N	Y	N
69	F	128	8	Y	N	N	Y	N	N	N	N	N
83	M	140	17	Y	Y	N	N	N	Y	Y	Y	Y
72	M	128	12	Y	Y	Y	N	N	Y	Y	Y	Y
65	M	120	2	Y	Y	N	Y	N	Y	N	Y	Y
70	F	120	NA	Y	Y	Y	Y	N	Y	Y	N	N
65	M	155	14	Y	Y	N	N	Y	N	Y	N	N
65	F	160	2	Y	Y	N	N	N	Y	N	N	N

Table 4. Individual characteristics of the ATH group: Y=Yes, N=No, NA=Not available. The Yes boxes are shaded for easier visual appraisal.
*A typical "white coat hypertensive", her readings ranged from 171 mmHg (on the day of measurements), through 150 mmHg with a doctor, down to 129 mmHg with a nurse.

APPENDIX II – EFFECT OF HYPERTENSION ON PPG DYNAMICS

To further investigate the signatures of ageing and treated hypertension in cardio-vascular regulation, we describe in this Appendix results obtained by phase-coherence analysis of pulse plethysmography (PPG) time series. The analyses and comparisons between groups were performed in the same way as for the laser Doppler flowmetry (LDF) time series discussed in the main text.

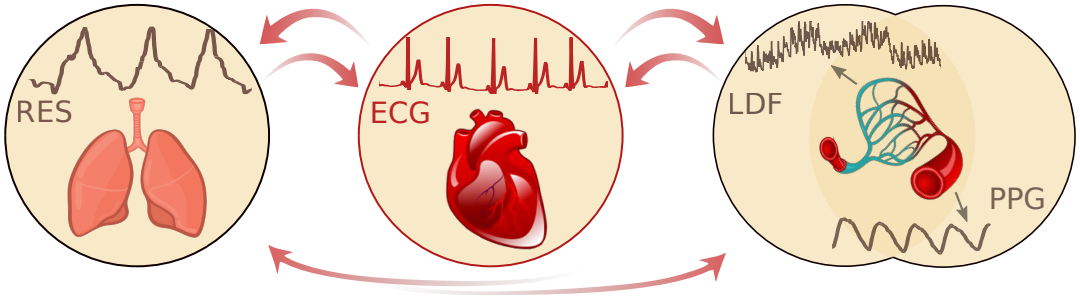

Figure 9. Schematic representation of the interactions between respiratory, cardiac and vascular activity, together with the corresponding recordings: respiratory effort signal (RES), electrocardiogram (ECG), laser Doppler flowmetry (LDF) and pulse plethysmography (PPG). In the resting state, the concentration of red blood cells can be considered constant, and so a Doppler shift in the velocity signal provides a measure of microvascular flow. In contrast, the finger PPG provides a measure of changes in arterial volume proportional to changes in arterial blood pressure.

Figure 9 illustrates schematically how both the LDF and the PPG data reflect the oscillations of the circulatory activity associated with different vascular levels, i.e. those of the capillary bed for LDF and those of the bigger vessels for PPG. The PPG was measured by a Finapress device (Omboni et al., 1993).

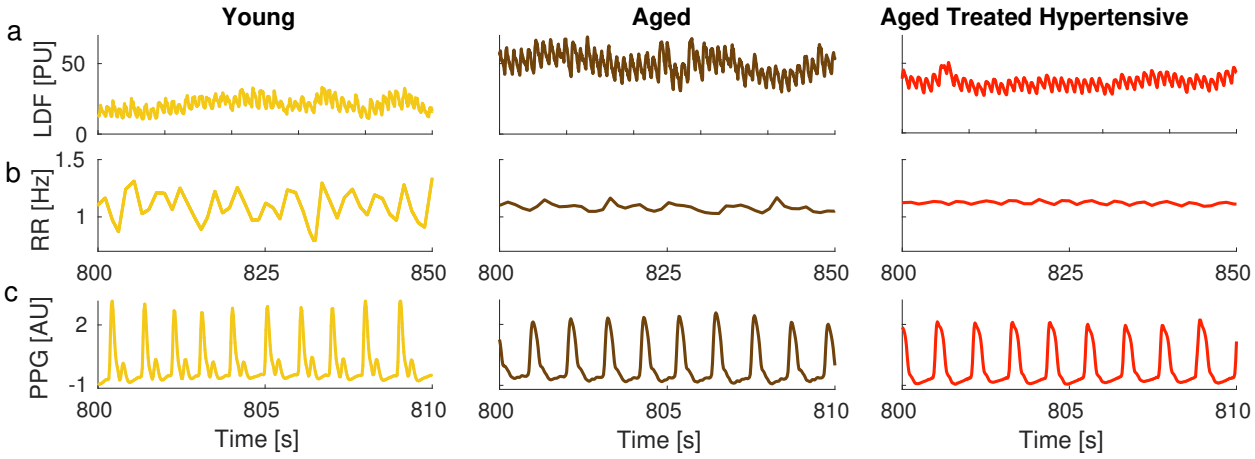

Figure 10. Typical time series: (a) Skin blood flow measured by the LDF (also referred to as SBF); (b) RR interval (RRI); and (c) PPG signals from each group of subjects. PU stands for perfusion units, and AU for arbitrary units

The different nature of the two signals is evident in Figure 10, where LDF, RR-interval and PPG time series are shown for a typical subject from each group: young (Y) in gold, aged (A) in brown, aged treated hypertensive (ATH) in red.

The coherence analyses are compared in Fig. 11, with RR-PPG in panels (a) and (b) and RR-LDF in (c) and (d). The results plotted in Fig. 11(b) and (d) show that for all groups there is significant coherence

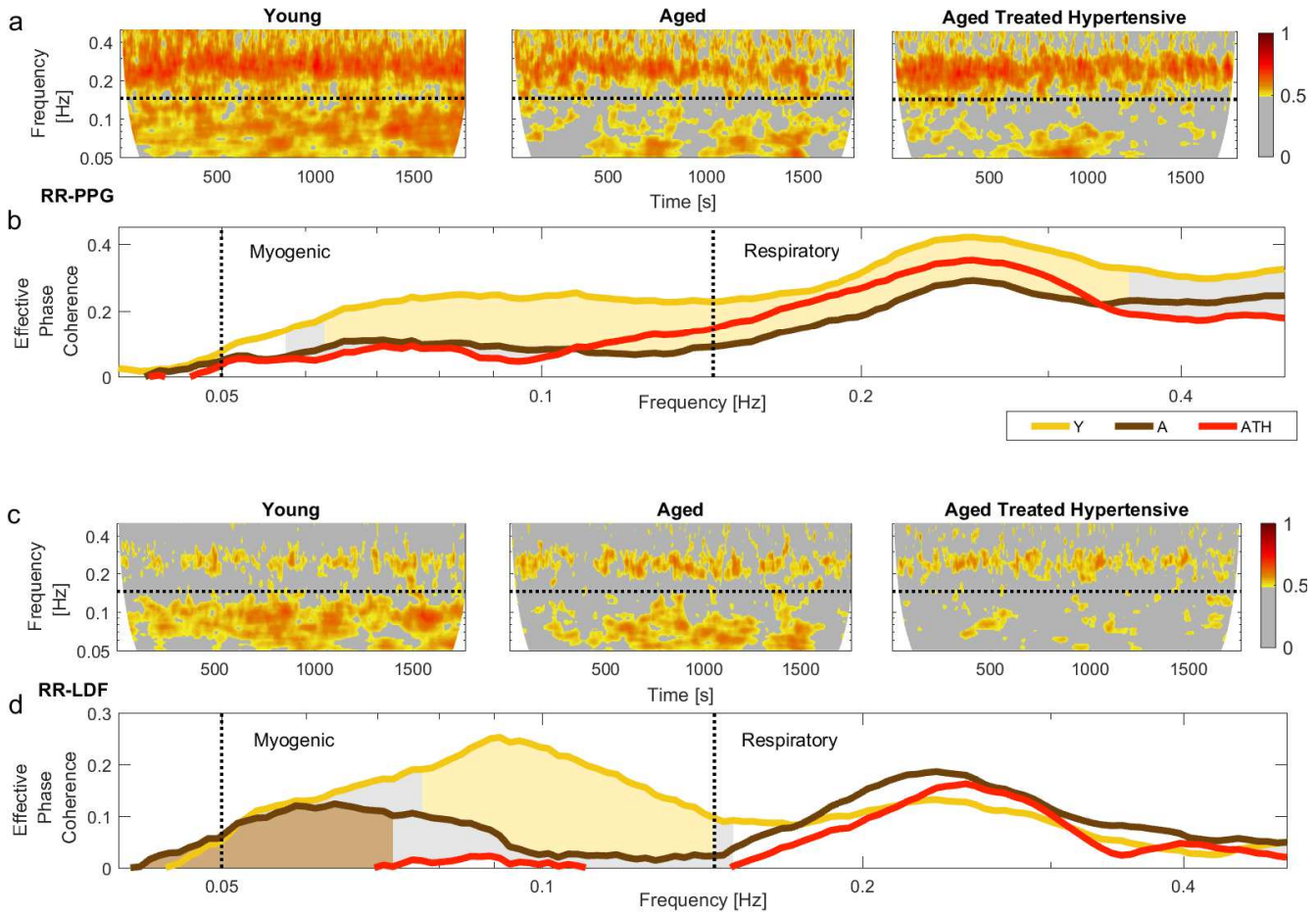

Figure 11. Comparison of RR-PPG, (a) and (b), with the corresponding RR-LDF, (c) and (d), phase coherences. Panels (a) and (c) show time-localised phase coherence obtained as a average for each group. Panels (b) and (d) show the time-averaged wavelet phase coherence (minus surrogate thresholds), and then averaged over groups; gold shading indicates significant difference between the Y and A groups, grey shading between Y and ATH, and brown shading between the A and ATH groups. Note how the coherence within the myogenic interval is higher in the Y than in the A and ATH groups in (b) and that it is diminished almost to vanishing point in the ATH group in (d).

(i.e. above the significance threshold) in the coherence of both PPG and LDF and the RR intervals in the respiratory and myogenic intervals.

For the PPG-RR coherence shown in Fig. 11(b), there is a significant difference between the Y and A (gold shading) and the Y and ATH groups (grey shading), but no significant difference between A and ATH. The similarity between A and ATH coherence, when compared to the Y pattern, also emerges from the time-localised group average in Fig. 11(a).

In contrast, the coherence between LDF and RR appears to decline with age, and it nearly disappears in treated hypertension, as illustrated in Fig. 11(d). Moreover, the comparison between A and ATH, which cannot be distinguished by the PPG-RR coherence, exhibits significant differences within the myogenic interval, as discussed in the main text. Fig. 11(c) presents the group-averaged time-localized coherence between RR intervals and blood flow.

These findings suggest that the LDF dynamics, which is a measure of the oscillatory patterns of capillary flow, is more sensitive to the effect of treated hypertension than PPG dynamics, probably because the latter reflects oscillations within bigger vessels.

REFERENCES

Aalkjaer, C., Boedtkjer, D., and Matchkov, V. (2011). Vasomotion – what is currently thought?, *Acta. Physiol.* 202, 253–269

Aalkjaer, C. and Nilsson, H. (2005). Vasomotion cellular background for the oscillator and for the synchronization of smooth muuscle cells, *Br. J. Pharmacol.* 144, 605–616

Agelink, M. W., Malessa, R., Baumann, B., Majewski, T., Akila, F., Zeit, T., and Ziegler, D. (2001). Standardized tests of heart rate variability: normal ranges obtained from 309 healthy humans, and effects of age, gender, and heart rate, *Clin. Autonom. Clin. Res.* 11, 99–108

Allen, J. (2007). Photoplethysmography and its application in clinical physiological measurement, *Physiol. Meas.* 28, R1–R39

Amaral, L. A. N., Goldberger, A. L., Ivanov, P. C., and Stanley, H. E. (1998). Scale-independent measures and pathologic cardiac dynamics, *Phys. Rev. Lett.* 81, 2388–2391

Antelmi, I., De Paula, R. S., Shinzato, A. R., Peres, C. A., Mansur, A. J., and Grupi, C. J. (2004). Influence of age, gender, body mass index, and functional capacity on heart rate variability in a cohort of subjects without heart disease, *Am. J. Cardiol.* 93, 381–385, doi:{10.1016/j.amjcard.2003.09.065}

Bahraminasab, A., Ghasemi, F., Stefanovska, A., McClintock, P. V. E., and Kantz, H. (2008). Direction of coupling from phases of interacting oscillators: A permutation information approach, *Phys. Rev. Lett.* 100, 084101

Bai, X., Lenhart, K. C., Bird, K. E., Suen, A. A., Rojas, M., Kakoki, M., Li, F., Smithies, O., Mack, C. P., and Taylor, J. M. (2013). The smooth muscle-selective RhoGAP GRAF3 is a critical regulator of vascular tone and hypertension, *Nat. Commun.* 4

Bandrivskyy, A., Bernjak, A., McClintock, P. V. E., and Stefanovska, A. (2004). Wavelet phase coherence analysis: Application to skin temperature and blood flow, *Cardiovasc. Engin.* 4, 89–93

Bashan, A., Bartsch, R. P., Kantelhardt, J. W., Havlin, S., and Ivanov, P. C. (2012). Network physiology reveals relations between network topology and physiological function, *Nat. Commun.* 3, 702

Bayes, T. (1763). An essay towards solving a problem in the doctrine of chances, *Phil. Trans. Roy. Soc. Lond.* 53, 370–418

Bernaola-Galván, P., Ivanov, P. C., Amaral, L. A. N., and Stanley, H. E. (2001). Scale invariance in the nonstationarity of human heart rate, *Phys. Rev. Lett.* 87, 168105

Bernardi, L., Hayoz, D., Wenzel, R., Passino, C., Calciati, A., Weber, R., and Noll, G. (1997). Synchronous and baroceptor-sensitive oscillations in skin microcirculation: evidence for central autonomic control, *Am. J. Physiol. - Heart. C.* 273, H1867–H1878

Bernjak, A., Cui, J., Iwase, S., Mano, T., Stefanovska, A., and Eckberg, D. L. (2012). Human sympathetic outflows to skin and muscle target organs fluctuate concordantly over a wide range of time-varying frequencies, *J. Physiol.* (London) 590, 363–375

Bertuglia, S., Colantuoni, A., Coppini, G., and Intaglietta, M. (1991). Hypoxia- or hyperoxia-induced changes in arteriolar vasomotion in skeletal muscle microcirculation, *Am. J. Physiol.* 260, H362–H372

Bertuglia, S., Colantuoni, A., and Intaglietta, M. (1994). Effects of L-NMMA and indomethacin on arteriolar vasomotion in skeletal-muscle microcirculation of conscious and anesthetized hamsters, *Microvasc. Res.* 48, 68–84

Billman, G. E. (2011). Heart rate variability – a historical perspective, *Front. Physiol.* 2, 86

Bollinger, A., Hoffmann, U., and Franzeck, U. K. (1991). Evalation of flux motion in man by the laser Doppler technique, *Blood Vessels.* 28, 21–26

Cevese, A., Gulli, G., Polati, E., Gottin, L., and Grasso, R. (2001). Baroreflex and oscillation of heart period at 0.1 Hz studied by α-blockade and cross-spectral analysis in healthy humans, *J. Physiol. (London)* 531, 235–244

Clemson, P., Lancaster, G., and Stefanovska, A. (2016). Reconstructing time-dependent dynamics, *Proc. IEEE* 104, 223–241

Clemson, P. T. and Stefanovska, A. (2014). Discerning non-autonomous dynamics, *Phys. Rep.* 542, 297–368

Colantuoni, A., Bertuglia, S., and Intaglietta, M. (1984a). Effects of anesthesia on the spontaneous activity of the microvasculature, *Int. J. Microcirc. Clin. Exp.* 3, 13–28

Colantuoni, A., Bertuglia, S., and Intaglietta, M. (1984b). Quantitation of rhythmic diameter changes in arterial microcirculation, *Am. J. Physiol.* 246, H508–H517

Duggento, A., Luchinsky, D. G., Smelyanskiy, V. N., Khovanov, I., and McClintock, P. V. E. (2008). Inferential framework for nonstationary dynamics. II. Application to a model of physiological signaling, *Phys. Rev. E* 77, 061106

Duggento, A., Stankovski, T., McClintock, P. V. E., and Stefanovska, A. (2012). Dynamical Bayesian inference of time-evolving interactions: From a pair of coupled oscillators to networks of oscillators, *Phys. Rev. E* 86, 061126

Ebert, T. J., Morgan, B. J., Barney, J. A., Denahan, T., and Smith, J. J. (1992). Effects of aging on baroreflex regulation of sympathetic activity in humans, *Am. J. Physiol. – Heart. C.* 263, H798–H803

Eckberg, D. L. (1997). Sympathovagal balance – A critical appraisal, *Circulation* 96, 3224–3232

Eckberg, D. L. (2003). The human respiratory gate, *J. Physiol. (London)* 548, 339–352

Feihl, F., Liaudet, L., Waeber, B., and Levy, B. I. (2006). Hypertension: A disease of the microcirculation?, *Hypertension* 48, 1012–1017

Furchgott, R. F. and Zawadzki, J. V. (1980). The obligatory role of endothelial cells in the relaxation of arterial smooth muscle by acetycholine, *Nature* 288, 373–376

Ghiadoni, L., Magagna, A., Versari, D., Kardasz, I., Huang, Y., Taddei, S., and Salvetti, A. (2003). Different effect of antihypertensive drugs on conduit artery endothelial function, *Hypertension* 41, 1281–1286

Goldberger, A. L., Amaral, L. A. N., Glass, L., Hausdorff, J. M., Ivanov, P. C., Mark, R. G., Mietus, J. E., Moody, G. B., Peng, C. K., and Stanley, H. E. (2000). PhysioBank, PhysioToolkit, and PhysioNet – Components of a new research resource for complex physiologic signals, *Circulation* 101, E215–E220

Guyenet, P. G. (2006). The sympathetic control of blood pressure, *Nature Rev. Neurosci.* 7, 335–346

Haddock, R. E. and Hill, C. E. (2005). Rhythmicity in arterial smooth muscle, *J. Physiol. (Lond.)* 566, 645–656

Hales, S. (1733). *Statical Essays, Containing Hæmastaticks, or, An Account of Some Hydraulick and Hydrostatical Experiments Made on the Blood and Blood Vessels of Animals. Vol. II*, London: Innys & Manby

Harvey, A., Montezano, A. C., and Touyz, R. M. (2015). Vascular biology of ageing? Implications in hypertension, *J. Mol. Cell. Cardiol.* 83, 112–121

Hoffman, U., Yanar, A., Franzeck, U. K., Edwards, J. M., and Bollinger, A. (1990). The frequency histogram – a new method for the evaluation of laser Doppler flux motion, *Microvasc. Res.* 40, 293–301

Iatsenko, D., Bernjak, A., Stankovski, T., Shiogai, Y., Owen-Lynch, P. J., Clarkson, P. B. M., McClintock, P. V. E., and Stefanovska, A. (2013). Evolution of cardio-respiratory interactions with age, *Phil. Trans. R. Soc. Lond. A* 371, 20110622

Iatsenko, D., McClintock, P. V. E., and Stefanovska, A. (2016). On the extraction of instantaneous frequencies from ridges in time-frequency representations of signals, *Signal Proc.* 125, 290–303

715 Iatsenko, D., Stefanovska, A., and McClintock, P. V. E. (2015). Nonlinear mode decomposition: a
716 noise-robust, adaptive, decomposition method, *Phys. Rev. E.* 92, 032916
717 Ivanov, P. C., Amaral, L. A. N., Goldberger, A. L., Havlin, S., Rosenblum, M. G., Stanley, H. E., and
718 Struzik, Z. R. (2001). From 1/f noise to multifractal cascades in heartbeat dynamics, *Chaos* 11, 641–652
719 Ivanov, P. C., Amaral, L. A. N., Goldberger, A. L., Havlin, S., Rosenblum, M. G., Struzik, Z. R., and
720 Stanley, H. E. (1999). Multifractality in human heartbeat dynamics, *Nature* 399, 461–465
721 Jamšek, J., Paluš, M., and Stefanovska, A. (2010). Detecting couplings between interacting oscillators with
722 time-varying basic frequencies: Instantaneous wavelet bispectrum and information theoretic approach,
723 *Phys. Rev. E* 81, 036207
724 Jensen-Urstad, K., Storck, N., Bouvier, F., Ericson, M., Lindblad, L. E., and JensenUrstad, M. (1997).
725 Heart rate variability in healthy subjects is related to age and gender, *Acta Physiol. Scand.* 160, 235–241
726 Jirsa, V. and Müller, V. (2013). Cross-frequency coupling in real and virtual brain networks, *Frontiers*
727 *Comput. Neurosci.* 7, 78
728 Johnson, P. C. (1991). The myogenic response, *News Physiol. Sci.* 6, 41–42
729 Julien, C. (2006). The enigma of Mayer waves: Facts and models, *Cardiovascular Research* 70, 12–21
730 Karstrup, J., Bühlow, J., and Lassen, N. A. (1989). Vasomotion in human-skin before and after local heating
731 recorded with laser Doppler flowmetry – A method for induction of vasomotion, *Int. J. Microcirc.: Clin.*
732 *Exp.* 8, 205–215
733 Kelly, R. I., Pearse, R., Bull, R. H., Leveque, J.-L., de Rigal, J., and Mortimer, P. S. (1995). The effects of
734 aging on the cutaneous microvasculature, *J. Am. Acad. Dermatol.* 33, 749–756
735 Kobayashi, M. and Musha, T. (1982). 1/f fluctuation of heartbeat period, *IEEE Trans. Biomed. Eng.* 29,
736 456–457
737 Kralemann, B., Frühwirth, M., Pikovsky, A., Rosenblum, M., Kenner, T., Schaefer, J., and Moser, M.
738 (2013). In vivo cardiac phase response curve elucidates human respiratory heart rate variability, *Nat.*
739 *Commun.* 4, 2418
740 Kralemann, B., Pikovsky, A., and Rosenblum, M. (2011). Reconstructing phase dynamics of oscillator
741 networks, *Chaos* 21, 025104
742 Kuramoto, Y. (1984). *Chemical Oscillations, Waves, and Turbulence*, Berlin: Springer-Verlag
743 Kvandal, P., Landsverk, S. A., Bernjak, A., Stefanovska, A., Kvernmo, H. D., and Kirkebøen, K. A. (2006).
744 Low frequency oscillations of the laser Doppler perfusion signal in human skin, *Microvasc. Res.* 72,
745 120–127
746 Kvandal, P., Stefanovska, A., Veber, M., Kvernmo, H. D., and Kirkebøen, K.-A. (2003). Regulation of
747 human cutaneous circulation evaluated by laser Doppler flowmetry, iontophoresis, and spectral analysis:
748 importance of nitric oxide and prostaglandines, *Microvasc. Res.* 65, 160–171
749 Kvernmo, H. D., Stefanovska, A., Bračič, M., Kirkebøen, K.-A., and Kvernebo, K. (1998). Spectral
750 analysis of the laser Doppler perfusion signal in human skin before and after exercise, *Microvasc. Res.*
751 56, 173–182
752 Landsverk, S. A., Kvandal, P., Bernjak, A., Stefanovska, A., and Kirkebøen, K. A. (2007). The effects of
753 general anesthesia on human skin microcirculation evalated by wavelet transform, *Anesth. Analg.* 105,
754 1012–1019
755 Landsverk, S. A., Kvandal, P., Kjelstrup, T., Benko, U., Bernjak, A., Stefanovska, A., Kvernmo, H., and
756 Kirkebøen, K. A. (2006). Human skin microcirculation after brachial plexus block evaluated by wavelet
757 transform of the laser Doppler flowmetry signal, *Anesthesiology* 105, 478–484
758 Levy, B. I. (2001). Artery changes with aging: degeneration or adaptation?, *Dialog. Cardiovas. Med.* 6,
759 104–111

760 Lotrič, M. B., Stefanovska, A., Štajer, D., and Urbančič-Rovan, V. (2000). Spectral components of heart
761 rate variability determined by wavelet analysis, *Physiol. Meas.* 21, 441–457
762 Ludwig, C. (1847). Beiträge zur Kenntniss des Einflusses der Respirationsbewegungen auf den Blutlauf im
763 Aortensysteme, *Arch. Anat. Physiol. wiss. Med.* 13, 242–302
764 Malik, M. (1996). Heart rate variability, *Ann. Noninvas. Electro.* 1, 151–181
765 Malliani, A., Pagani, M., Lombardi, F., and Cerutti, S. (1991). Cardiovascular neural regulation explored in
766 the frequency domain, *Circulation* 84, 482–492
767 Malpas, S. C. (2002). Neural influences on cardiovascular variability: possibilities and pitfalls, *Am. J.*
768 *Physiol.: Heart. Circ. Physiol.* 282, H6–H20
769 McCurley, A., Pires, P. W., Bender, S. B., Aronovitz, M., Zhao, M. J., Metzger, D., Chambon, P., Hill,
770 M. A., Dorrance, A. M., Mendelsohn, M. E., and Jaffe, I. Z. (2012). Direct regulation of blood pressure
771 by smooth muscle cell mineralocorticoid receptors, *Nat. Med.* 18, 1429–1435
772 Messaoudi, S., He, Y., Gutsol, A., Wight, A., Hébert, R. L., Vilmundarson, R. O., Makrigiannis, A. P.,
773 Chalmers, J., Hamet, P., Tremblay, J., et al. (2015). Endothelial Gata5 transcription factor regulates
774 blood pressure, *Nat. Commun.* 6
775 Mormann, F., Lehnertz, K., David, P., and Elger, C. E. (2000). Mean phase coherence as a measure for
776 phase synchronization and its application to the eeg of epilepsy patients, *Physica D* 144, 358–369
777 NBP-Lancaster (2016). Collection of Matlab toolboxes, http://py-biomedical.lancaster.ac.uk/
778 Omboni, S., Parati, G., Frattola, A., Mutti, E., Di Rienzo, M., Castiglione, P., and Mancia, G. (1993).
779 Spectral and sequence analysis of finger blood pressure variability. comparison with analysis of intra-
780 arterial recordings, *Hypertension* 22, 26–33
781 Pagani, M., Lombardi, F., Guzzetti, S., Rimoldi, O., Furlan, R., Pizzenelli, P., Sandrone, G., Malfatto,
782 G., Dellorto, S., Piccaluga, E., Turiel, M., Baselli, G., Cerutti, S., and Malliani, A. (1986). Power
783 spectral-analysis of heart-rate and arterial-pressure variabilities as a marker of sympathovagal interaction
784 in man and conscious dog, *Circulation Res.* 59, 178–193
785 Paluš, M. and Stefanovska, A. (2003). Direction of coupling from phases of interacting oscillators: An
786 information-theoretic approach, *Phys. Rev. E* 67, 055201(R)
787 Pikovsky, A., Rosenblum, M., and Kurths, J. (2001). *Synchronization – A Universal Concept in Nonlinear*
788 *Sciences*, Cambridge: Cambridge University Press
789 Rosenblum, M. G. and Pikovsky, A. S. (2001). Detecting direction of coupling in interacting oscillators,
790 *Phys. Rev. E.* 64, 045202
791 Rossi, M., Bradbury, A., Magagna, A., Pesce, M., Taddei, S., and Stefanovska, A. (2011). Investiga-
792 tion of skin vasoreactivity and blood flow oscillations in hypertensive patients: effect of short-term
793 antihypertensive treatment, *J. Hypertens.* 29, 1569–1576
794 Rossi, M., Carpi, A., Di Maria, C., Galetta, F., and Santoro, G. (2006). Spectral analysis of laser Doppler
795 skin blood flow oscillations in human essential arterial hypertension, *Microvasc. Res* 72, 34–41
796 Saul, J. P., Berger, R. D., Albrecht, P., Stein., S. P., Chen, M. H., and Cohen, R. J. (1991). Transfer
797 function analysis of the circulation – unique insights into cardiovascular regulation, *Am. J. Physiol.* 261,
798 H1231–H1245
799 Schmidt, J. A., Intaglietta, M., and Borgstom, P. (1992). Periodic hemodynamics in skeletal-muscle during
800 local arterial-pressure reduction, *J. Appl. Physiol.* 73, 1077–1083
801 Sheppard, L. W., Stefanovska, A., and McClintock, P. V. E. (2012). Testing for time-localised coherence in
802 bivariate data, *Phys. Rev. E* 85, 046205
803 Shiogai, Y., Stefanovska, A., and McClintock, P. V. E. (2010). Nonlinear dynamics of cardiovascular
804 ageing, *Phys. Rep.* 488, 51–110

Smelyanskiy, V. N., Luchinsky, D. G., Stefanovska, A., and McClintock, P. V. E. (2005). Inference of a nonlinear stochastic model of the cardiorespiratory interaction, *Phys. Rev. Lett.* 94, 098101

Söderström, T., Stefanovska, A., Veber, M., and Svenson, H. (2003). Involvement of sympathetic nerve activity in skin blood flow oscillations in humans, *Am. J. Physiol.: Heart. Circ. Physiol.* 284, H1638–H1646

Sörös, P., Whitehead, S., Spence, J. D., and Hachinski, V. (2013). Antihypertensive treatment can prevent stroke and cognitive decline, *Nat. Rev. Neurol.* 9, 174–178

Stankovski, T., Duggento, A., McClintock, P. V. E., and Stefanovska, A. (2012). Inference of time-evolving coupled dynamical systems in the presence of noise, *Phys. Rev. Lett.* 109, 024101

Stankovski, T., McClintock, P. V. E., and Stefanovska, A. (2014a). Coupling functions enable secure communications, *Phys. Rev. X* 4, 011026

Stankovski, T., McClintock, P. V. E., and Stefanovska, A. (2014b). Dynamical inference: Where phase synchronization and generalized synchronization meet, *Phys. Rev. E* 89, 062909

Stankovski, T., Pereira, T., McClintock, P. V. E., and Stefanovska, A. (2017a). Coupling functions: Universal insights into dynamical interaction mechanisms, *Rev. Mod. Phys.* in press *arXiv preprint* `https://arxiv.org/abs/1706.01810`

Stankovski, T., Ticcinelli, V., McClintock, P. V. E., and Stefanovska, A. (2015). Coupling functions in networks of oscillators, *New J. Phys.* 17, 035002

Stankovski, T., Ticcinelli, V., McClintock, P. V. E., and Stefanovska, A. (2017b). Neural cross-frequency coupling functions, *Front. Syst. Neurosci.* 11, 10.3389/fnsys.2017.00033

Stauss, H. M., Anderson, E. A., Haynes, W. G., and Kregel, K. C. (1998). Frequency response characteristics of sympathetically mediated vasomotor waves in humans, *Am. J. Physiol.: Heart. Circ. Physiol.* 274, H1277–H1283

Stefanovska, A. (2007). Coupled oscillators: Complex but not complicated cardiovascular and brain interactions, *IEEE Eng. Med. Bio. Magazine* 26, 25–29

Stefanovska, A. and Bračič, M. (1999). Physics of the human cardiovascular system, *Contemp. Phys.* 40, 31–55

Stefanovska, A., Bračič, M., and Kvernmo, H. D. (1999). Wavelet analysis of oscillations in the peripheral blood circulation measured by laser Doppler technique, *IEEE Trans. Bio. Med. Eng.* 46, 1230–1239

Stefanovska, A., Haken, H., McClintock, P. V. E., Hožič, M., Bajrović, F., and Ribarič, S. (2000). Reversible transitions between synchronization states of the cardiorespiratory system, *Phys. Rev. Lett.* 85, 4831–4834

Stefanovska, A. and Hožič, M. (2000). Spatial synchronization in the human cardiovascular system, *Prog. Theor. Phys.* Supple. 139, 270–282

Taddei, S. and Bruno, R. M. (2016). Endothelial dysfunction in hypertension: achievements and open questions, *J. Hypertens.* 34, 1492–1493

Taddei, S., Virdis, A., Ghiadoni, L., Sudano, I., and Salvetti, A. (2000). Antihypertensive drugs and reversing of endothelial dysfunction in hypertension, *Curr. Hypertens. Rep.* 2, 64–70

Toledo, E., Akselrod, S., Pinhas, I., and Aravot, D. (2002). Does synchronization reflect a true interaction in the cardiorespiratory system?, *Med. Eng. & Phys.* 24, 45–52

Varela, F., Lachaux, J.-P., Rodriguez, E., and Martinerie, J. (2001). The brainweb: phase synchronization and large-scale integration, *Nat. Rev. Neurosci.* 2, 229–239

Verdecchia, P., Porcellati, C., Schillaci, G., Borgioni, C., Ciucci, A., Battistelli, M., Guerrieri, M., Gatteschi, C., Zampi, I., and Santucci, A. (1994). Ambulatory blood pressure. An independent predictor of prognosis in essential hypertension, *Hypertension* 24, 793–801

Virdis, A., Savoia, C., Grassi, G., Lembo, G., Vecchione, C., Seravalle, G., and Rizzoni, D. (2014). Evaluation of microvascular structure in humans: 'a state-of-the-art' document of the Working Group on Macrovascular and Microvascular Alterations of the Italian Society of Arterial Hypertension, *J. Hypertens.* 32, 2120–2129

von Toussaint, U. (2011). Bayesian inference in physics, *Rev. Mod. Phys.* 83, 943–999

Wilting, J. and Lehnertz, K. (2015). Bayesian inference of interaction properties of noisy dynamical systems with time-varying coupling: capabilities and limitations, *Eur. Phys. J. B* 88, 1–11

World Health Organisation (2013). *A Global Brief on Hypertension: Silent Killer, Global Public Health Crisis*, Geneva: WHO Publications

Xie, L., Liu, B., Wang, X., Mei, M., Li, M., Yu, X., and Zhang, J. (2017). Effects of different stresses on cardiac autonomic control and cardiovascular coupling, *J. Appl. Physiol.* 122, 435–445

Yannoutsos, A., Levy, B. I., Safar, M. E., Slama, G., and Blacher, J. (2014). Pathophysiology of hypertension: interactions between macro and microvascular alterations through endothelial dysfunction, *J. Hypertens.* 32, 216–224